[American Journal of Science, Vol. 319, May, 2019, P. 339-380, DOI 10.2475/05.2019.01]

American Journal of Science

MAY 2019

THE THERMOCHRONOLOGIC RECORD OF EROSION AND MAGMATISM IN THE CANYONLANDS REGION OF THE COLORADO PLATEAU

KENDRA E. MURRAY*,†, PETER W. REINERS*, STUART N. THOMSON*, XAVIER ROBERT**, and KELIN X WHIPPLE***

ABSTRACT. The Cenozoic history of crustal deformation, surface uplift, and erosion of the central Colorado Plateau (southwestern USA) is distinct from and relatively poorly understood compared with surrounding regions in the North American Cordillera, including the Grand Canyon region and the southwestern Plateau margin. Here, we present new apatite thermochronologic results from Paleozoic-Mesozoic sandstones sampled in the Canyonlands region—the interior of the Colorado Plateau in southeastern Utah. The apatite (U-Th-Sm)/He (He) ages are highly dispersed, with both positive-slope and negative-slope age-effective U (eU) trends. Samples with apatite He results suitable for thermal history modeling are from the Abajo and La Sal mountains intrusive complexes and the Permian, Triassic, and Jurassic rocks sampled near the Colorado River at Lees Ferry, Arizona, and Hite, Utah. Samples with the richest thermal history information have positive-slope apatite He age-[eU] trends, with ages *ca.* 10 to 5 Ma at [eU] < 10 ppm and *ca.* 25 to 20 Ma at [eU] > 60 ppm. Modeled thermal histories that best predict this pattern require two periods of rock cooling: one during the middle Cenozoic *ca.* 30 to 20 Ma and the other since the latest Miocene *ca.* 6 Ma. The most recent cooling documents the transition from a slowly eroding Miocene landscape to recent rapid erosion that likely postdates 6 Ma and the integration of the modern Colorado River. Middle Cenozoic rock cooling can be attributed to either ~1 km of erosion between *ca.* 25 and 15 Ma, as previous workers have suggested in other parts of the Colorado Plateau region, or relaxation of a geothermal gradient transiently doubled by magmatism associated with the vigorous magmatic flare-up that swept through the region *ca.* 34 to 20 Ma. The ambiguity of using middle Cenozoic rock cooling as a proxy for erosion in this region means that this event should be described using a nongenetic term: the Middle Cenozoic Cooling Event.

Keywords: Colorado Plateau, apatite thermochronology, (U-Th)/He age variability, erosion, flare-up magmatism, middle Cenozoic rock cooling

INTRODUCTION

Deciphering the geodynamic history of eroded landscapes like the Colorado Plateau (fig. 1) is challenging because erosion destroys the physical geologic record. Even with excellent exposures of distinctive Paleozoic and Mesozoic strata, which offered early workers a guide to the total amount of rock removed from the Plateau by Cenozoic erosion (Powell, 1875; Dutton, 1882; Emmons, 1897), it was not until the development of low-temperature thermochronology a century later that it became

*Department of Geosciences, University of Arizona, Tucson, Arizona, USA
**Université Grenoble Alpes, CNRS, IRD IFSTARR, ISTerre, Grenoble, France
***School of Earth and Space Exploration, Arizona State University, Tempe, Arizona, USA
†Corresponding author, currently at Hamilton College Department of Geosciences, Clinton, New York: kemurray@hamilton.edu

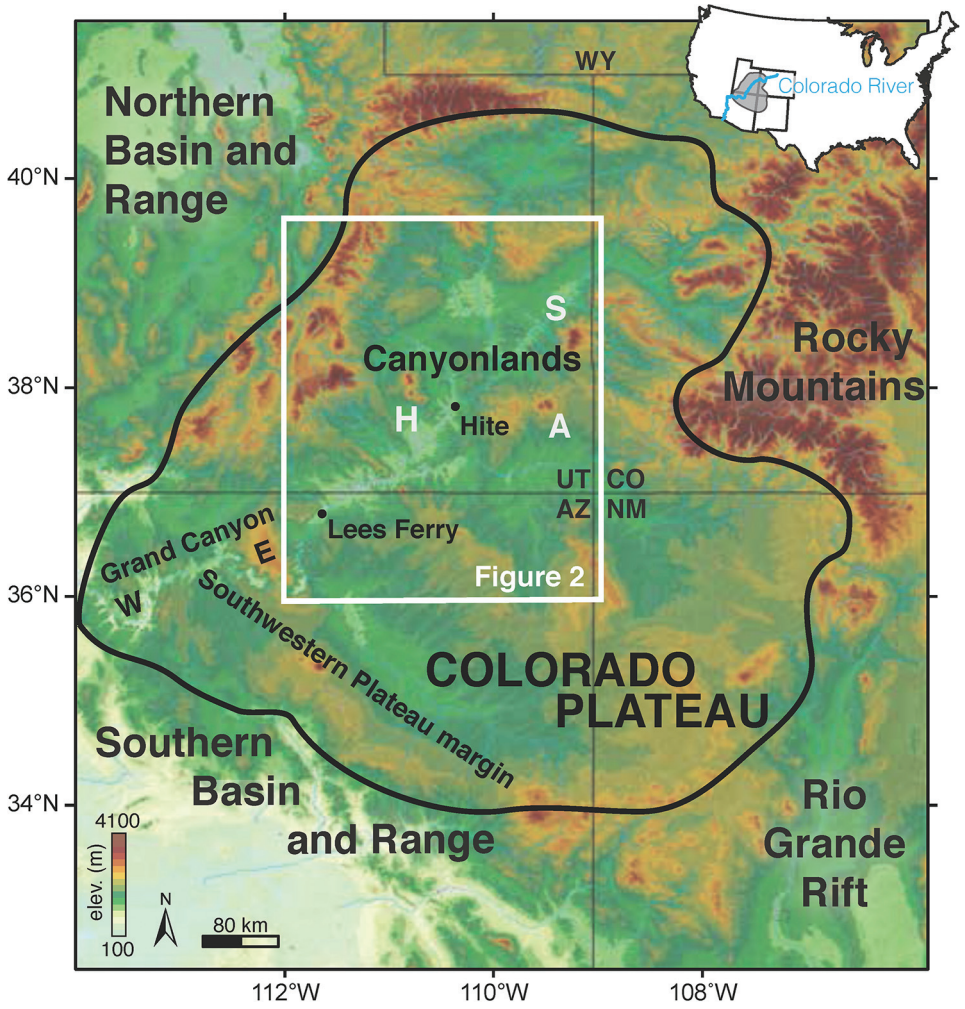

Fig. 1. Digital elevation map of the Colorado Plateau and surrounding regions in the southwestern USA. H—Henry Mountains; LS—La Sal Mountains; A—Abajo Mountains.

possible to infer the spatial and temporal scales of erosion itself—using rock cooling as a proxy for exhumation. Along with other advances, apatite fission-track (AFT; temperature sensitivity 140–90 °C, Green and others, 1989; Ketcham and others, 2007) and apatite (U-Th-Sm)/He (He; temperature sensitivity 90–45 °C, Farley, 2000; Flowers and others, 2009) thermochronology has spurred a resurgence in studies of the Colorado Plateau (Flowers and others, 2008; Wernicke, 2011; Karlstrom and others, 2012; Braun and others, 2013; Lee and others, 2013; Karlstrom and others, 2014; Winn and others, 2017) because the erosion history of the region is one of the few ways to test or constrain the various hypotheses regarding the cryptic Cenozoic history of this iconic landscape (Morgan and Swanberg, 1985; Spencer, 1996; McQuarrie and Chase, 2000; Pederson and others, 2002; Moucha and others, 2009; Humphreys, 2009; Levander and others, 2011; Roy and others, 2009).

It is now widely accepted that the Colorado Plateau region experienced three periods of rock cooling documented by apatite thermochronology: Late Cretaceous to

early Paleogene, middle Cenozoic, and latest Miocene to Recent (Dumitru and others, 1994; Flowers and others, 2008; Hoffman, ms, 2009; Hoffman and others, 2011; Wernicke, 2011; Flowers and Farley, 2012; Kelley and Karlstrom, 2012; Lee and others, 2013; Fox and Shuster, 2014; Karlstrom and others, 2014). The oldest cooling dominates the low-temperature history of rocks from the southwestern margin of the Plateau, including the Western Grand Canyon, whereas the youngest cooling dominates the Plateau interior (fig. 1; for example, Flowers and others, 2008). The interpretation of these cooling ages is controversial because datasets of the thermochronologic system sensitive to the lowest temperatures, apatite He, exhibit substantial inter- and intra-sample single-grain age variability (that is to say, dispersion) that is challenging to interpret. In the Grand Canyon region, this He age variability inspired widely applicable advances in our understanding of how radiation damage in apatite grains controls the diffusivity of He and the resulting cooling ages (Flowers and others, 2007; Flowers and others, 2009; Gautheron and others, 2009). These data also stimulated a vigorous argument about how to model and interpret the thermal histories of samples from the Grand Canyon region (Wernicke, 2011; Flowers and Farley, 2012; Lee and others, 2013; Fox and Shuster, 2014; Karlstrom and others, 2014; Flowers and others, 2015; Fox and others, 2017; Winn and others, 2017). In the Plateau interior northeast (and upstream) of the Grand Canyon in southeastern Utah (called the Canyonlands region by Hunt, 1956), dispersed apatite He ages have also made thermal history interpretations difficult (Hoffman, ms, 2009; Murray and others, 2014). Additional data are needed to fill important geographic gaps and to better understand the thermochronologic record here and how it pertains to the region's Cenozoic history.

We present new results from the Canyonlands region (fig. 2) that enrich our understanding of the processes documented by apatite thermochronology from the Colorado Plateau. A new suite of samples of Permian-Cretaceous sandstones collected in a transect from the Vermilion Cliffs near Lees Ferry, Arizona, to the mesas northeast of Hite, Utah, fill a >200 km gap in apatite thermochronologic data along the upper Colorado River corridor (fig. 3A). This transect is complemented by additional samples of Permian-Cretaceous sandstones from the thermal aureoles around Oligocene plutons in the La Sal and Abajo mountains. Localized heating from this plutonic activity, which was part of a larger flare-up in regional magmatism (Johnson, 1991; Lipman and Glazner, 1991; Best and others, 2009; Best and others, 2016), is an independently constrained Oligocene thermal event useful for modeling the Neogene-Recent thermal history of these sedimentary rocks (for example, Murray and others, 2016).

Apatite He results from both sample suites are dominated by highly variable single-grain ages (>20 % standard deviation on sample mean age). Recent work on the sources of apatite He age variability (for example, Flowers and Kelley, 2011) allows us to distinguish samples useful for thermal history interpretations—with reproducible ages or age variability consistent with the known coevolution of radiation damage and He diffusivity in apatite (Flowers and others, 2009; Gautheron and others, 2009)—from those that suffer from additional, currently intractable, sources of age dispersion (Spiegel and others, 2009). Samples from our study area with age trends suitable for thermal history modeling document rock cooling during both middle Cenozoic and latest Miocene-Recent time. Middle Cenozoic cooling in sandstone samples from the Oligocene plutonic complexes is likely the localized, postmagmatic cooling around shallow plutons purposefully targeted for this study. In contrast, middle Cenozoic cooling in samples far (>20 km) from the intrusive complexes could be the result of erosion, as has been reported previously for the south-central Colorado Plateau (Flowers and others,

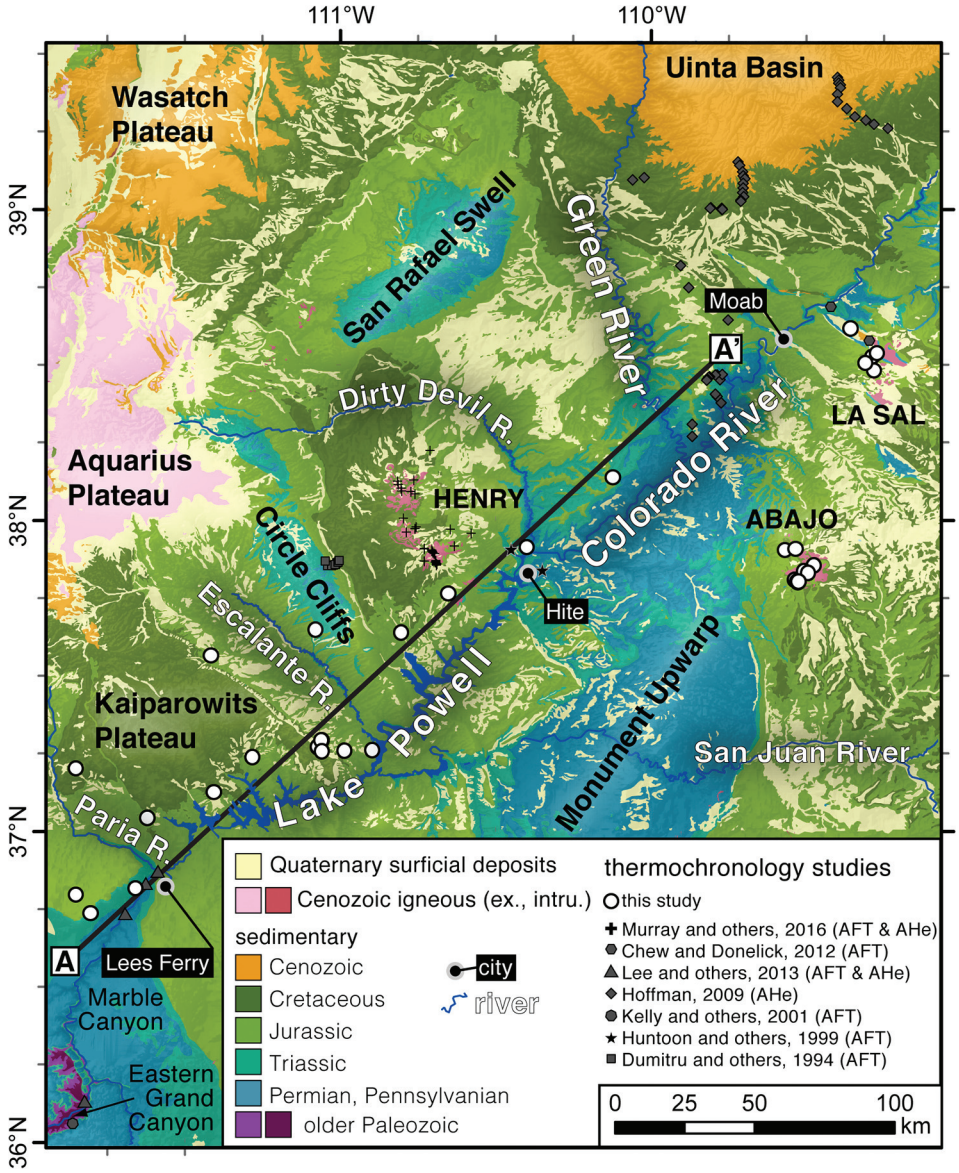

Fig. 2. Simplified geologic map of the study region (modified from Hintze and others, 2000) with the locations of the apatite thermochronology samples from this study (white circles) and previous studies. Sample locations are projected along the A to A' transect in figure 3.

2008; Karlstrom and others, 2017) and Eastern Grand Canyon (Lee and others, 2013). Alternatively, this middle Cenozoic cooling may document transient changes in the regional geothermal gradient during the magmatic flare-up (Murray and others, 2018). Here, we evaluate the geologic evidence for middle Cenozoic erosion in the Canyonlands region and use thermal history and simple 1D thermal models to test whether it is possible to distinguish between magmatic and exhumational cooling with these thermochronologic data.

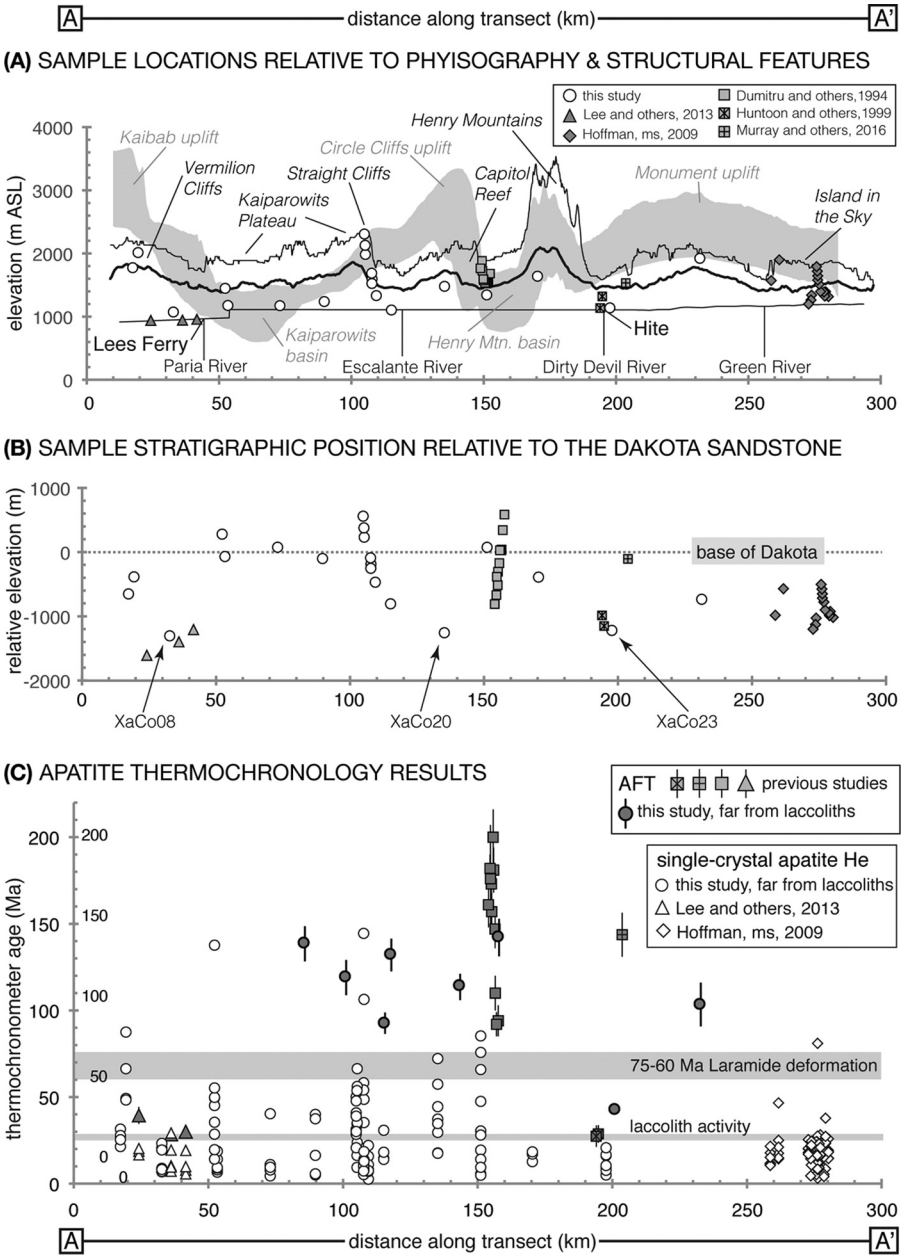

Fig. 3. Thermochronology samples and results from this and previous studies in the context of the topographic and structural features from A to A' in figure 2. Samples from the Henry (Murray and others, 2016), La Sal, and Abajo mountains (this study) are not plotted. (A) Sample elevation vs. distance along the A to A' transect with an approximately 25× vertical exaggeration. Black lines are the mean (thick), maximum, and minimum surface elevations from a DEM swath from the Colorado River and a region ~50 km NW of the river. The minimum elevation along this swath profile is the Colorado River. The gray field is a swath profile of the base of the Cretaceous Dakota Sandstone from the same ~50-km-wide region, as contoured by Bump and Davis (2003), which shows long-wavelength variability in the elevation of the Colorado Plateau stratigraphy. Black labels identify physiographic features. Light gray labels identify structure features. Thermochronology sample locations from this and previous studies are projected onto this transect. The step in the river profile upstream of Lees Ferry is the Glen Canyon Dam. (B) Thermochronology sample locations vs. their elevation relative to the base of the Dakota Sandstone. (C) Thermochronometer age vs. distance from A to A'.

GEOLOGIC SETTING

The Colorado Plateau (fig. 1) is an ~350,000 km^2 province of Proterozoic lithosphere (Bowring and Karlstrom, 1990) covered by a 3 to 5 km veneer of mostly Phanerozoic sediments, which indicate that this region was at or near sea level until Late Cretaceous time. At that time, the Colorado Plateau was part of the foreland basin of the Sevier Orogeny, the convergent orogenic system that built the Sierra Nevada batholith, the extensive Sevier thin-skinned fold and thrust belt, and a high-elevation orogenic plateau (DeCelles, 2004; Cassel and others, 2012). The end of foreland marine sedimentation during the Late Cretaceous corresponds with the beginning of the Laramide Orogeny, when there was a fundamental shift in the style and position of crustal shortening and magmatism in this region. The Laramide is commonly attributed to a period of shallow or flat subduction of the Farallon slab that subsequently re-steepened in middle Cenozoic time (Armstrong, 1974; Dickinson and Snyder, 1978; Humphreys, 1995; English and others, 2003; Humphreys and others, 2003; Liu and others, 2010; Jones and others, 2011; Copeland and others, 2017). During and after the Laramide Orogeny, the Rocky Mountain and Basin and Range provinces (fig. 1) experienced extensive crustal deformation and voluminous magmatism as a result of the region's protracted transition from mature convergent orogen to collapsed transform plate boundary. Meanwhile, sometime during the Cenozoic, the rocks and surface of the Colorado Plateau uplifted from sea level to ~2 km above sea level without voluminous volcanism or the extensive crustal deformation that commonly drives rock uplift of this magnitude.

Cenozoic Shortening

During the Laramide Orogeny, the laterally continuous retroarc foreland basin and marine shelf east of the Sevier thrust belt fragmented into discrete sedimentary basins bounded by basement-cored uplifts of various scales and orientations (Dickinson and others, 1988). In the Colorado Plateau region, isolated Laramide uplifts and monoclines folded the Paleozoic and Mesozoic stratigraphy (Bump and Davis, 2003) and controlled the local fluvial and lacustrine systems that developed in the wake of the final regression of the Late Cretaceous seaway (Elston and Young, 1991; Goldstrand, 1994; Davis and others, 2009). Laramide sediments are preserved in basins at the northwestern, northern, and southwestern edges of the Plateau (Dickinson and others, 1988; Davis and others, 2009) but not in our study area (fig. 2). An erosional response to Laramide shortening in the Grand Canyon region and along the southwestern margin of the Colorado Plateau is documented by early Cenozoic thermochronologic cooling ages (Naeser and others, 1989; Dumitru and others, 1994; Flowers and others, 2008; Kelley and Karlstrom, 2012; Lee and others, 2013; Karlstrom and others, 2014; Karlstrom and others, 2017) and preserved paleocanyons and canyon fill (Elston and Young, 1991; Dumitru and others, 1994; Young, 2001; Young and Hartman, 2014). AFT ages from the Waterpocket fold (Circle Cliffs uplift, fig. 3) may document some early Cenozoic erosion at the crest of a Laramide uplift in the Plateau interior and Canyonlands region (Dumitru and others, 1994). The Uinta Mountains uplift at the northern edge of the Plateau experienced significant Paleogene erosion (Carroll and others, 2006).

Cenozoic Magmatism

Magmatism swept inboard from the Sierra Nevada arc as far east as the Colorado Mineral Belt in the southern Rocky Mountains at *ca.* 75 Ma. Together with the complementary eastward sweep of crustal shortening, this event is thought to track flattening of the subducting Farallon slab (Snyder and others, 1976; Coney and Reynolds, 1977; Dickinson and Snyder, 1978; Chapin, 2012; Copeland and others, 2017). From the latest Cretaceous to Eocene time, arc magmatism continued in the

Idaho batholith to the north of the Colorado Plateau region and Mexican Cordillera to the south (Armstrong and Ward, 1991), but there was a lull in magmatic activity at Colorado Plateau latitudes (Dickinson and Snyder, 1978; Copeland and others, 2017). At *ca.* 40 Ma, magmatic activity began to sweep back toward the west, likely following the rollback of the Farallon flat slab (Best and Christiansen, 1991; Humphreys and others, 2003; Farmer and others, 2008; Best and others, 2016). By the end of Oligocene time, regional magmatism had grown into one of the largest productions of silicic magma in the geologic record (Johnson, 1991; Best and others, 2009). This magmatic flare-up erupted ~500,000 km^3 of volcanic rock across southwestern North America (Johnson, 1991; Lipman and Glazner, 1991; Best and others, 2009; Best and others, 2016).

The Colorado Plateau was surrounded by large silicic eruptive centers during the middle Cenozoic magmatic flare-up. The San Juan volcanic field at the eastern edge of the Plateau erupted 25,000 km^3 of intermediate and 16,000 km^3 of ignimbrite lava, most *ca.* 29 to 26.9 Ma (Lipman, 2007; Farmer and others, 2008; Lake and Farmer, 2015). The Marysvale volcanic complex at the western edge of the Plateau erupted 12,000 km^3 of material *ca.* 26 to 23 Ma (Rowley and others, 1998). The Mogollon-Datil volcanic field at the southeastern Plateau edge erupted 6,000 km^3 of lava, mostly in a large pulse *ca.* 29.1 to 27.4 Ma (McIntosh and others, 1992; Davis and others, 1993).

The only evolved Cenozoic igneous rocks in the Colorado Plateau interior are the comparatively small Oligocene intrusive complexes of the Henry, La Sal, and Abajo mountains (Hunt and others, 1953; Hunt, 1958; Witkind, 1964; Nelson and others, 1992; Nelson and Davidson, 1993). The potassic, xenolith-bearing maar-diatreme volcanoes of the Navajo field in the Four Corners region southeast of Canyonlands are also coeval with the ignimbrite flare-up (Roden and others, 1979; Laughlin and others, 1986; Semken, 2003). Following the middle Cenozoic flare-up, magmatism in the Colorado Plateau region was restricted to small-volume mafic dikes, lava flows, and cinder cones (Gonzales and Lake, 2017) erupted mainly at the western and southern Plateau margins (Roy and others, 2009; Van Wijk and others, 2010; Crow and others, 2011).

Plateau Uplift

A range of competing, but not mutually exclusive, models have been proposed for the surface uplift of the Colorado Plateau. These models include (1) Paleogene uplift driven by the Laramide flat slab changing the buoyancy of the Colorado Plateau lithosphere via hydration (Spencer, 1996; Humphreys and others, 2003; Jones and others, 2015; Porter and others, 2017), crustal flow (Bird, 1984; McQuarrie and Chase, 2000), or dynamic effects (Liu and Gurnis, 2010); (2) middle Cenozoic uplift driven by buoyancy changes from lithospheric foundering (Bird, 1979), basaltic melt extraction during the magmatic flare-up (Roy and others, 2004), or lithospheric hydration (Schulze and others, 2015; Porter and others, 2017); and (3) Neogene uplift related to progressive post-Laramide warming of the lithosphere (Roy and others, 2009) or dynamic uplift driven by mantle upwelling (Moucha and others, 2009; Liu and Gurnis, 2010; Braun and others, 2013). A component of uplift is likely an isostatic response to Cenozoic erosion (Pederson and others, 2002). Given the complex and evolving tectonic setting, the surface uplift history of the Colorado Plateau likely has multiple phases and drivers. Paleoelevation estimates for the Grand Canyon region, though likely blurred by Cenozoic climate variability, support kilometer-scale Paleogene surface uplift of the southwestern Plateau margin (Huntington and others, 2010).

Thermochronology has been used to infer the surface uplift history of the Colorado Plateau (for example, Flowers and others, 2008), but such work requires two assumptions. The first assumption is that the rock thermal histories document erosional exhumation and not rock cooling resulting from changes in the crustal thermal

field (for example, Dumitru and others, 1991; House and others, 2003 and our considerations here). The second is that the rock uplift induced a temporally associated and measurable erosional response. In this study, we focus explicitly on thermal and erosion histories inferred from thermochronology results and do not infer insights regarding the surface uplift history of the Plateau.

The Colorado River and Late Cenozoic Erosion

The modern Colorado River flows from the western Rocky Mountains and through the Canyonlands of the central Colorado Plateau, cutting across Laramide structures and through the Grand Canyon before entering the Basin and Range *en route* to the Pacific basin. Although the mechanisms for the integration of the river remain controversial (for example, Dickinson, 2013), the timing is clear: the modern Colorado River did not deliver sediment to the basins downstream of the Grand Canyon until the latest Miocene *ca.* 5.3 Ma (Dorsey and others, 2007), and since that time an enormous volume of sediment has been transported off the Plateau and deposited in the transtensional basins of the San Andreas fault system (Dorsey and Lazear, 2013; Lazear and others, 2013; Kimbrough and others, 2015). This river integration accompanied a substantial base-level drop from the Plateau interior to the Basin and Range province, and this change in base-level is the principal candidate driver of the subsequent erosion of the Colorado River headwaters. Erosion rates in the central Colorado Plateau region since the late Miocene may be unsteady and reflect transient response(s) to river integration modulated by knickpoint migration and response to variable rock strength (Cook and others, 2009; Darling and others, 2012; Pederson and Tressler, 2012; Bursztyn and others, 2015), feedback between erosion and isostatic rebound (Lazear and others, 2013; Pederson and others, 2013), and possibly upper mantle dynamics (Karlstrom and others, 2012).

STUDY AREA

The Canyonlands region of the Colorado Plateau in southeastern Utah encompasses an extensive network of canyons occupied by the modern Colorado River and its tributaries (figs. 1 and 2). The samples in this study, with the exception of those from the Vermilion Cliffs near Marble Canyon and Lees Ferry, are from the Upper Colorado River Basin and upstream of a lithologic boundary at Lees Ferry that likely affected the erosional responses to base-level fall when the river integrated through the Grand Canyon (Cook and others, 2009). The orientation of this upstream-dipping boundary is the result of the Kaibab uplift, one of several Laramide monoclines with wavelengths of 50 to 100 km that control the elevation of the Permian-Cretaceous strata (fig. 2). The most extensive areas of significant erosion of the Mesozoic stratigraphy—where the deepest parts of the stratigraphic section are exposed—are on the crests of the Laramide uplifts and deep in the canyons of the Colorado River system (figs. 2 and 3A). Paleozoic sediments also crop out in contact with the laccoliths in the Henry, Abajo, and La Sal mountains. The entire pre-Laramide Permian-Cretaceous stratigraphy, at least up though the Mancos Shale and its equivalent units, are preserved in the Henry Mountains, Kaiparowits, and Unita Laramide structural basins; in the Henry, La Sal, and Abajo mountains intrusive complexes; and in the mesas along the Colorado-Utah border (fig. 2). This preservation permits the confident reconstruction of the thickness of this sedimentary sequence across the study area. Therefore, the presence or absence of the Mesozoic strata and their current elevation above sea level are useful measures of the total rock uplift and exhumation since the Late Cretaceous (fig. 3A).

The Henry, La Sal, and Abajo mountains (figs. 1 and 2) are Oligocene intrusive complexes (Gilbert, 1877; Hunt, 1958; Witkind, 1964; Nelson and others, 1992) comprising groups of sills, dikes, and laccoliths up to ~5 km in diameter, which

uplifted and folded the sedimentary cover rocks during emplacement (Gilbert, 1877; Johnson and Pollard, 1973; Pollard and Johnson, 1973; Jackson and Pollard, 1988).

Previous low-temperature thermochronology from the Canyonlands region (fig. 2) includes AFT results from the Waterpocket fold that may reflect some Late Cretaceous erosional exhumation of the Circle Cliffs uplift followed by moderate reheating in middle Cenozoic time (Dumitru and others, 1994). Other AFT results include two ~28 Ma ages from Permian sandstones near Hite (Huntoon and others, 1999) and river-level samples in the Permian sandstones from the Lees Ferry-Marble Canyon region that are 28 to 39 Ma (Kelley and Karlstrom, 2012). Modeling of AFT and He results from the Lees Ferry region supports rock cooling in both middle and late Cenozoic time (Lee and others, 2013) and suggests that Marble Canyon was carved in the last *ca.* 6 Ma (Karlstrom and others, 2014). AFT results from the La Sal Mountains laccoliths document rapid postmagmatic thermal relaxation to colder than partial-annealing temperatures (Rønnevik and others, 2017). The only apatite He cooling ages from the central Colorado Plateau Canyonlands prior to this study suggest an onset or acceleration of erosion in the late Miocene (*ca.* 10–4 Ma, Hoffman, ms, 2009; Hoffman and others, 2011). Additionally, thermal history modeling of sandstones sampled from the thermal aureole of the Henry Mountains intrusive complex document little-to-no Neogene erosion until after 5 Ma (Murray and others, 2016).

METHODS

We collected surface bedrock samples from Permian-Cretaceous sandstones exposed across the central Colorado Plateau and from the plagioclase-hornblende diorite porphyries that core the intrusive complexes in the Abajo and La Sal mountains in southeastern Utah (table 1, figs. 2 and 3A). Apatite and zircon grains were separated from each sample using standard crushing, density, and magnetic separation methods. Additional methodology information is available in the Appendix. We provide the complete geochronologic and thermochronologic analyses in the supplementary data tables (http://earth.geology.yale.edu/%7eajs/SupplementaryData/2019/Murray). All age errors are $\pm 2\sigma$ unless otherwise noted.

We collected samples for AFT and He thermochronology along a NE-SW-trending transect from the Vermilion Cliffs near Lees Ferry in northern Arizona to the mesas northeast of Hite, Utah. This work fills a >200 km gap in apatite He data along the main stem of the Colorado River between the Eastern Grand Canyon and the confluence with the Green River in Canyonlands (figs. 2 and 3). In addition, we sampled in the Abajo and La Sal intrusive complexes because previous work in the Henry Mountains demonstrated the utility of dating detrital apatite grains from Paleozoic-Mesozoic sandstones that likely experienced a localized middle Cenozoic heating event (Murray and others, 2016). In the Abajo and La Sal mountain ranges, we used a multichronometer approach to evaluate the timing and extent of heating and cooling related to the local magmatic activity. Zircon U-Pb and AFT dating of the shallow diorite porphyries documents the timing of magmatic activity and the timing and extent of postmagmatic cooling, respectively.

U-Pb geochronology of zircon grains from the La Sal and Abajo mountains diorite porphyries was conducted by laser ablation multicollector inductively coupled plasma mass spectrometry (LA-MC-ICP-MS) at the Arizona LaserChron Center using an Element 2 ICP-MS and following the methods of Gehrels and others (2008). Weighted mean $^{206}Pb/^{238}U$ ages reported with the analyses in supplementary data table 1 were calculated using the routines in Isoplot (Ludwig, 2008). Final uncertainties were determined by quadratic addition of the weighted mean and external uncertainties.

For AFT analysis, samples were analyzed by applying the external detector method (Gleadow, 1981). Central ages (Galbraith, 1981), presented with 1σ errors in table 2, were calculated using the IUGS recommended zeta calibration approach of Hurford

TABLE 1

Sample information and summary of apatite He results

Sample	Latitude (°N)	Longitude (°W)	Elev (m)	Locale	Rock type	Formation	Depo age	Apatite He summary				Other ages
								#	Ages (Ma)	S.D. %	[eU] (ppm)	
Laccolith mountain ranges												
Abajo Mountains												
12ABA01	37.7960	-109.5247	2553	Johnson Creek dome	porphyry	Scrub Oak laccolith	N.A.	6	13-28 (33)	30%	8-51	Zrc U-Pb
12ABA03	37.8006	-109.5306	2712	Johnson Creek dome	sandstone	Moss Back, Chinle	Triassic	4	16-30	25%	16-92	N.A.
12ABA04	37.7983	-109.5287	2623	Johnson Creek dome	sandstone	Shinarump, Chinle	Triassic	N.D.	N.D.	N.D.	N.D.	AFT
12ABA05	37.8018	-109.5364	2754	Johnson Creek dome	porphyry	Prospect laccolith	N.A.	6	18-26	15%	4-24	Zrc U-Pb
12ABA07	37.8978	-109.5669	2453	Shay Ridge Road	sandstone	Dakota	Cretaceous	4	15-21	14%	27-94	N.A.
12ABA08	37.9015	-109.5343	2207	Shay Ridge Road	sandstone	Navajo	Jurassic	8	6-12	23%	16-51	AFT
12ABA09	37.8488	-109.4742	3057	North Creek Road	porphyry	Abajo Peak laccolith	N.A.	5	17-32	26%	3-9	Zrc U-Pb
12ABA10	37.8304	-109.5067	3006	Jackson Ridge	porphyry	Jackson Ridge laccolith	N.A.	3	13-30	39%	4-26	Zrc U-Pb
12ABA13	37.7938	-109.5263	2433	Johnson Creek dome	sandstone	Cutler Group	Permian	12	11-30 (43)	41%	9-197	N.A.
12ABA14	37.7954	-109.5290	2464	Johnson Creek dome	sandstone	Cutler Group	Permian	10	11-27	23%	3-106	AFT
12ABA15	37.8234	-109.4926	2691	North Creek Road	sandstone	Morrison	Jurassic	12	7-40	52%	7-38	N.A.
La Sal Mountains												
10SAL01	38.4735	-109.2815	2891	Middle Mountain	porphyry	Brumbly Ridge laccolith	N.A.	6	14-27	23%	16-43	Zrc U-Pb, AFT
10SAL02	38.5181	-109.2865	2706	Schuman Gulch	sandstone	Dakota	Cretaceous	6	11-19	20%	9-146	AFT
10SAL03	38.4991	-109.3086	2374	Mill Creek	sandstone	Salt Wash, Morrison	Jurassic	12	8-24	25%	7-57	AFT
10SAL05	38.5303	-109.2719	3340	Miners Basin	porphyry	Gold Knob laccolith	N.A.	N.D.	N.D.	N.D.	N.D.	Zrc U-Pb, AFT
12SAL02	38.6109	-109.3579	1721	Castle Valley	porphyry	Round Mountain	N.A.	N.D.	N.D.	N.D.	N.D.	Zrc U-Pb
Canyonlands transect												
XaCo06	36.7295	-111.8031	1775	Vermillion Cliffs	sandstone	Moenkopi	Triassic	6	21-32	13%	11-81	N.A.
XaCo08	36.8088	-111.6563	1073	Vermillion Cliffs	sandstone	Moenave	Triassic	7	7-23	54%	9-129	N.A.
XaCo09	36.7885	-111.8480	2015	Vermillion Cliffs	sandstone	Glen Canyon Group	Jurassic	4	48-88	29%	15-34	N.A.
XaCo10	37.1950	-111.8483	1448	Kaiparowits Plateau	sandstone	Straight Cliffs	Cretaceous	9	14-138	75%	5-141	N.A.
XaCo11	37.0366	-111.6203	1177	Kaiparowits Plateau	sandstone	Entrada	Jurassic	10	7-19	38%	8-30	N.A.
XaCo37	37.1177	-111.4052	1321	Kaiparowits Plateau	sandstone	Dakota	Cretaceous	8	5-40	91%	10-24	AFT
XaCo38	37.2321	-111.2815	1239	Kaiparowits Plateau	sandstone	Morrison	L. Jurassic	5	5-40	81%	7-59	AFT
XaCo12	37.5575	-111.4159	1596	Straight Cliffs	sandstone	Entrada	Jurassic	4	13-106	78%	14-87	N.A.
XaCo14	37.2519	-110.9853	1333	Straight Cliffs	sandstone	Entrada	Jurassic	9	4-81	132%	1-37	N.A.
XaCo15	37.2862	-111.0576	1525	Straight Cliffs	sandstone	Morrison	Jurassic	8	8-20	35%	5-35	N.A.
XaCo16	37.2635	-111.0698	2130	Straight Cliffs	sandstone	Straight Cliffs	Cretaceous	4	9-54	70%	6-31	N.A.
XaCo17	37.2647	-111.0698	1985	Straight Cliffs	sandstone	Straight Cliffs	Cretaceous	6	15-66	48%	6-64	N.A.
XaCo18	37.2862	-111.0591	1688	Straight Cliffs	sandstone	Morrison	L. Jurassic	10	1-144	144%	2-85	AFT
XaCo40	37.2499	-111.0567	2308	Straight Cliffs	sandstone	Straight Cliffs	Cretaceous	8	21-50	28%	10-134	AFT
XaCo39	37.2542	-110.8950	1105	Escalante confluence	sandstone	Navajo	Jurassic	4	14-31	40%	8-25	N.A.
XaCo20	37.6421	-111.0770	1480	Circle Cliffs	sandstone	Chinle	L. Triassic	8	18-72	49%	9-69	AFT
XaCo21	37.6319	-110.8014	1344	Henry Mtn. basin	sandstone	Salt Wash, Morrison	L. Jurassic	11	5-85	83%	1-42	AFT
XaCo22	37.7570	-110.6512	1640	Mount Ellsworth	sandstone	Entrada	Jurassic	4	13-18	16%	7-101	N.A.
XaCo23	37.9060	-110.3979	1139	Hite	sandstone	Cedar Mesa	Permian	8	5-21 (300)	46%	14-116	AFT
XaCO25	38.1203	-110.1258	1966	The Maze	sandstone	Wingate	E. Jurassic	N.D.	N.D.	N.D.	N.D.	AFT

TABLE 2

Apatite Fission Track data

Sample	# crystals	Track Density ($x10^6$ tr cm^{-2}) ρ_s (N_s)	ρ_i (N_i)	ρ_d (N_d)	Mean Dpar (μm)	Age Dispersion ($P\chi^2$)	Central Age (Ma ± 1σ)	Mean Track Length (μm ± 1 s.e.) (no. of tracks)	s.d. (μm)
Abajo Mountains									
sandstone samples									
12 ABA 04	7	0.2699 (52)	0.924 (178)	0.9634 (3083)	3.05	<0.01% (87.8%)	51.6 ± 8.5	-	-
12 ABA 08	5	0.1953 (11)	0.1101 (62)	0.9558 (3058)	1.94	<0.01% (28.7%)	31.1 ± 10.3	-	-
12 ABA 14	20	0.7102 (205)	0.2654 (765)	0.9482 (3034)	2.17	<0.01% (97.1%)	46.5 ± 4.2	14.43 ± 0.14 (59)	1.05
La Sal Mountains									
porphyry samples									
10 SAL 01	20	0.1375 (121)	1.251 (1101)	1.251 (4003)	2.11	<0.01% (99.8%)	25.3 ± 2.9	-	-
10 SAL 05	14	0.0991 (38)	0.8215 (315)	1.216 (3891)	2.07	<0.01% (98.1%)	26.9 ± 4.8	-	-
sandstone samples									
10 SAL 02	20	0.1511 (96)	1.279 (813)	1.239 (3966)	2.35	<0.01% (99.9%)	26.9 ± 3.1	-	-
10 SAL 03	14	0.1329 (66)	1.186 (589)	1.228 (3928)	2.43	<0.01% (93.3%)	25.3 ± 3.5	-	-
Transect									
Xa CO 18	20	0.4624 (340)	0.839 (617)	1.244 (3982)	2.66	0.1% (75.9%)	125.0±10.0 mixed age?	13.42±0.24 (38)	1.44
Xa CO 20	20	1.183 (412)	2.536 (883)	1.23 (3937)	2.08	4.9% (32.2%)	105.0±7.9 mixed age	12.72±0.28 (43)	1.84
Xa CO 21	20	0.4129 (334)	0.6848 (554)	1.216 (3891)	2.73	9.6% (31.9%)	135.7±11.7 mixed age	13.95±0.31 (22)	1.4
Xa CO 23 sum	60	0.3658 (610)	2.816 (4695)	1.188 (3800)	1.95	<0.01% (99.9%)	28.4±1.7	13.65±0.38 (22)	1.72
Xa CO 23	*20*	*0.37 (211)*	*2.787 (1589)*	*1.202 (3846)*	*2.1*	*<0.01% (99.9%)*	*29.3±2.5*	-	-
Xa CO 23A	*20*	*0.349 (128)*	*2.656 (974)*	*1.188 (3800)*	*1.87*	*<0.01% (99.9%)*	*28.7±3.0*	-	-
Xa CO 23B	*20*	*0.3711 (271)*	*2.92 (2132)*	*1.173 (3754)*	*1.88*	*<0.01% (99.9%)*	*27.4±2.1*	-	-
Xa CO 25	10	1.327 (124)	2.975 (278)	1.158 (3709)	2.15	24.8% (14.9%)	93.9±13.8 mixed age	-	-
Xa CO 37	20	0.5646 (348)	0.8924 (550)	1.145 (3663)	2.6	3.6% (48.6%)	131.8±10.8 mixed age	13.64±0.23 (46)	1.54
Xa CO 38	20	0.5419 (292)	0.9928 (535)	1.131 (3618)	2.73	19.7% (15.7%)	110.9±10.9 mixed age	13.72±0.23 (28)	1.21
Xa CO 40	20	0.6822 (403)	1.7 (1004)	1.116 (3572)	1.97	13.3% (29.0%)	82.3±6.7 mixed age	12.16±0.27 (42)	1.73

and Green (1983). AFT analysis and length data were limited by low track densities and the small grain size common in the sandstones sampled. The complete AFT results for each sample are available in supplementary data table 2.

We selected individual apatite grains for apatite He analysis under a 120-160x stereo-zoom microscope based on size, clarity, morphology, and the lack of visible inclusions or grain boundary phases (GBPs, Murray and others, 2014). A minimum of four grains were selected per sample and as many as 15 to 20 grains were dated from samples with apparently useful age variability. Dimensions of each dated grain were measured from digital photographs and used to calculate the alpha-ejection (F_T) correction (Ketcham and others, 2011). U, Th, and Sm contents of each grain were measured by isotope dilution and solution ICP-MS on an Element 2 ICP-MS, as described by Reiners and others (2004) and Reiners (2005). The complete apatite He results for each grain dated are available in supplementary data table 3.

To interpret the apatite He results, we used the 1σ standard deviation on the sample mean age to determine whether each sample had reproducible ages (<20 %) or dispersed ages (that is to say, variable, overdispersed, or apparently reproducible ages; ≥20 %; Flowers and Kelley, 2011; table 1). To interpret the cooling ages of samples with variable He ages, we plotted single-grain ages against two known—and useful—sources of age variability: grain effective U (eU) concentration ([eU]=[U]+0.235[Th]) and grain size (Flowers and Kelley, 2011). Dispersed samples with no apparent correspondence between He age and grain [eU] and/or size have age variability that is not useful for thermal history interpretations given our current understanding of these systems (Flowers and Kelley, 2011). In contrast, dispersed samples with a positive-slope age-[eU] trend and sufficient range of [eU] (at least ~10 ppm to >30 ppm) contain robust thermal history information. We built thermal history models for the samples with apatite He data useful for thermal history analysis using the radiation damage accumulation and annealing model (RDAAM, Flowers and others, 2009) as implemented in the program HeFTy (v. 1.9.3, Ketcham, 2005). Thermal history modeling details are described below and in the Appendix. We jointly modeled the results with AFT data where available.

RESULTS

Laccolith-cored Mountain Ranges

Abajo Mountains.—Four porphyry samples from the Abajo Mountains intrusive complex have a weighted mean zircon U-Pb age of 27.8 ± 0.16 Ma (supplementary data table 1). To our knowledge, these are the first zircon U-Pb analyses from the Abajo Mountains. This result agrees with but is significantly more precise than previous hornblende K-Ar and $^{40}Ar/^{39}Ar$ age determinations (Witkind, 1964; Armstrong, 1969; Nelson and others, 1992). Dated zircon grains have abundant Proterozoic inherited cores (supplementary data table 1). Although not the focus of this study, we note that most of these cores have ages of *ca.* 1.44 to 1.38 Ga, similar to xenocryst ages abundant in xenoliths from the nearby Oligocene Navajo Volcanic field (Condie and others, 1999; Crowley and others, 2006). Curiously, the oldest ages in the inherited cores are 1.68 to 1.6 Ga (that is, Mazatzal) and not 1.8 to 1.7 Ga (that is, Yavapai) as would be expected based on a strictly vertical projection of the inferred configuration of the basement terranes (Bowring and Karlstrom, 1990).

AFT ages from three sandstone samples have middle Cenozoic central ages younger than the depositional age but older than 28 Ma (table 2). Sample 12ABA08 from the Navajo sandstone exposed at the northern end of the range near Shay Mountain has an AFT central age of 31.1 ± 10.3 Ma (1σ). The sample had only five datable grains, leading to high age uncertainty, but the age is within error of the crystallization age of the intrusive complex. Sample 12ABA04 from the Chinle Formation exposed in the Johnson Creek dome is 51.6 ± 8.5 Ma (1σ). Sample 12ABA14, also from the Johnson Creek dome, is from the Organ Rock Member of the Cutler Group and has a central age of 46.5 ± 4.2 Ma (1σ) and long track lengths of 14.41 ± 0.14 μm (n=59).

The apatite He ages from four Oligocene porphyry samples in the Abajo Mountains are 33.0 to 12.7 Ma, with three ages older than 28 Ma (table 1, fig. 4). Like apatite grains from the coeval Henry Mountains porphyries (Murray and others, 2016), these apatite grains have low [eU] values (mostly <20 ppm) and significantly dispersed ages. The youngest single-grain apatite He ages from the porphyry samples are middle Miocene and all younger than the magmatic activity in the Abajo Mountains intrusive complex.

The apatite He ages from five Permian-Cretaceous sandstones also have significant intra-sample age variability, and most ages are <28 Ma (table 1, fig. 4). At the

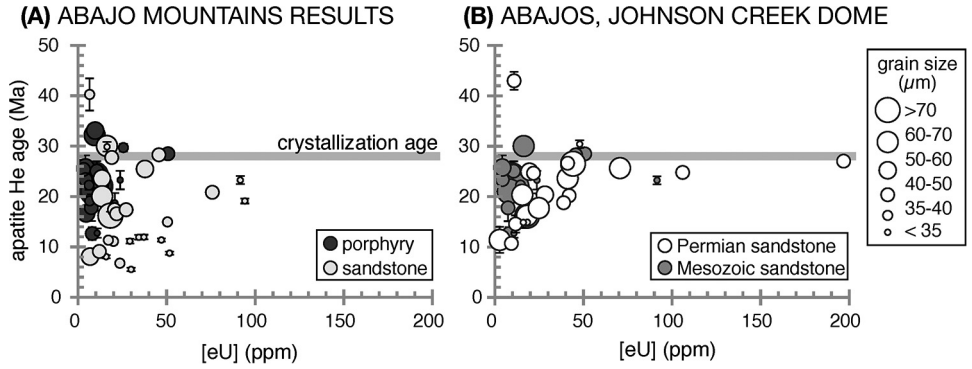

Fig. 4. Apatite He results from the Abajo Mountains diorite porphyries and their sedimentary country rocks. Symbols are scaled to apatite grain size (the effective spherical radius). (A) Most samples have single-grain age variability at low apatite [eU] (<50 ppm) that results in an overall wedge-shaped trend. (B) Results from Johnson Creek dome, the most deeply exhumed part of the intrusive complex. Ages from Permian Sandstones (white circles) have a positive-slope age-[eU] trend with a steep change in ages from 10 to ~25 Ma in apatite grains with [eU] from 5 to 50 ppm, and a flat age-[eU] plateau at ~25 Ma for apatite grains with up to 200 ppm [eU].

northern end of the Abajo Mountains study area, Cretaceous Dakota Sandstone has reproducible He ages 20.8 to 15.0 Ma (12ABA07). The Jurassic Navajo Sandstone in this area, which is lower stratigraphically and in elevation, has younger variable ages (11.9–5.5 Ma, 12ABA08) from apatite grains that were smaller and lower in [eU] than those from the Dakota Sandstone (fig. 4A). The Jurassic Morrison Formation at Jackson Ridge (12ABA15) has ages 40.0 to 6.8 Ma. At the Johnson Creek dome (fig. 4B), where lower Triassic and upper Permian rocks are exposed in contact with the Prospect laccolith, ages range from 43.0 to 10.7 Ma. Unlike the other sandstone samples, these samples—especially two from the Permian Cutler Group—have positive-slope age-[eU] trends with ages of 25 to 11 Ma at [eU] values of <50 ppm and an ~27 to 25 Ma age plateau at [eU] values of 50 to 200 ppm (fig. 4B).

La Sal Mountains.—Two porphyry samples from the La Sal Mountains intrusive complex, North Mountain and Round Mountain (Castle Valley) localities, have a weighted mean zircon U-Pb age of 27.7 ± 0.21 Ma (fig. 5A, supplementary data table 1). This result is consistent with previous K-Ar, hornblende $^{40}Ar/^{39}Ar$, and zircon U-Pb age determinations (Stern and others, 1965; Armstrong, 1969; Nelson and others, 1992) and slightly younger than recently published zircon U-Pb ages of 29.1 ± 0.3 Ma from Middle Mountain (Rønnevik and others, 2017). As in the Abajo Mountains, Proterozoic inherited cores are abundant (supplementary data table 1).

The AFT ages from four samples, two porphyry and two sandstone samples, are younger than, but within error of, the zircon U-Pb crystallization age of the La Sal Mountains intrusive complex (table 2, fig. 5A) They have central ages from 26.9 ± 4.8 Ma to 25.3 ± 3.5 Ma (1σ). This range agrees with the 33 to 27 Ma AFT ages reported by Rønnevik and others (2017).

The apatite He ages from three samples are 26.7 to 8.3 Ma (table 1, fig. 5), with significant intra-sample age variability. Minimum He ages young with decreasing elevation (fig. 5A). The highest-elevation sample is a porphyry with ages from 27.6 to 14 Ma that are positively correlated with grain size. The other two samples, from the Upper Jurassic Dakota Sandstone and the Salt Wash Member of the Morrison Formation, have positive-slope age-[eU] trends (fig. 5B), with 10 to 7 Ma ages at [eU] values < 10 ppm and an 18 to 17 Ma age plateau at [eU] values of 25 to 150 ppm.

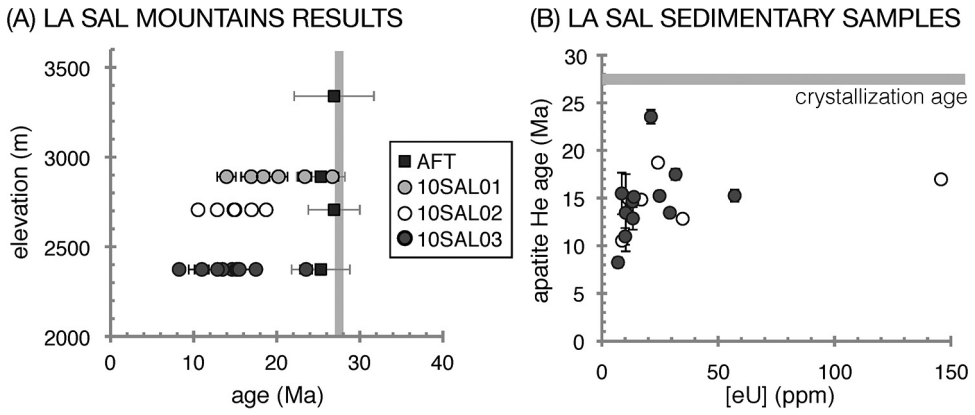

Fig. 5. Apatite thermochronology results from the La Sal Mountains diorite porphyries and their sedimentary country rocks. (A) Sample elevation vs. thermochronologic age. The vertical gray bar is the zircon U-Pb age of porphyry samples 10SAL05 and 10SAL01. (B) Apatite He age vs. [eU] plot for the two sandstone samples.

Lees Ferry to Hite Transect

Nineteen samples from Permian-Cretaceous sandstones collected along the Colorado River corridor (fig. 2) lie along a transect that cuts several Laramide structural highs and lows (fig. 3A). AFT results vary as a function of stratigraphic level and proximity to Laramide structures (table 2, fig. 6). Cretaceous and Upper Jurassic strata have depositional and older AFT ages, whereas older Jurassic, Triassic, and Permian strata have partially reset Late Cretaceous central ages at the deeply exhumed cores of Laramide structures or fully reset Oligocene ages along the Colorado River corridor far from Laramide structural highs. All He ages from these samples, with the exception of seven (of 131) grains, are Cenozoic and significantly younger than the deposition age of the sampled units. There is significant inter- and intra-sample apatite He age variability. Before addressing this He age variability, we present the results by geographic region.

Vermilion Cliffs near Lees Ferry.—Three samples form an ~1 km vertical profile up the Vermilion Cliffs (figs. 3A and 7A). These samples sit on the northeastern side of the Kaibab uplift and have a systematic age-elevation pattern (fig. 7A). The highest-elevation sample (2015 m) is from the Jurassic Kayenta Formation, and has four apatite He ages from 87 to 48 Ma with a steep and positive-slope age-[eU] pattern over a narrow range of [eU] values from 15 to 34 ppm (fig. 7B; XaCo09). In the middle of this profile (1775 m), a sample from the Triassic Moenkopi Sandstone has ages from 32 to 21 Ma with a large range of apatite eU compositions (11–81 ppm; XaCo06; fig. 7B). The lowest-elevation samples, taken from the Triassic Moenave Formation on the Marble Platform (1073 m) has apatite He ages from 23.2 to 6.8 Ma that have a positive-slope age-[eU] pattern over [eU] values from 9 to 129 ppm (fig. 7B; XaCo08). Lee and others (2013) presented apatite He data from river-level samples ~100 m lower in Marble Canyon that have the same age range and age-[eU] patterns as this Moenave sample.

Straight Cliffs.—This vertical profile samples a similar range of elevations as the Vermilion Cliffs profile, but the units are higher in the stratigraphic section because they sit in the Kaiparowits structural basin (figs. 3A, 3B, and 7C). All samples have at least one He age younger than 25 Ma. The highest-elevation sample, from the Upper Cretaceous Straight Cliffs Formation (2308 m) has apatite He ages from 50 to 20 Ma and an AFT age of 82.3 ± 6.7 Ma (±1σ; XaCo40; fig. 7C). This sample also has a

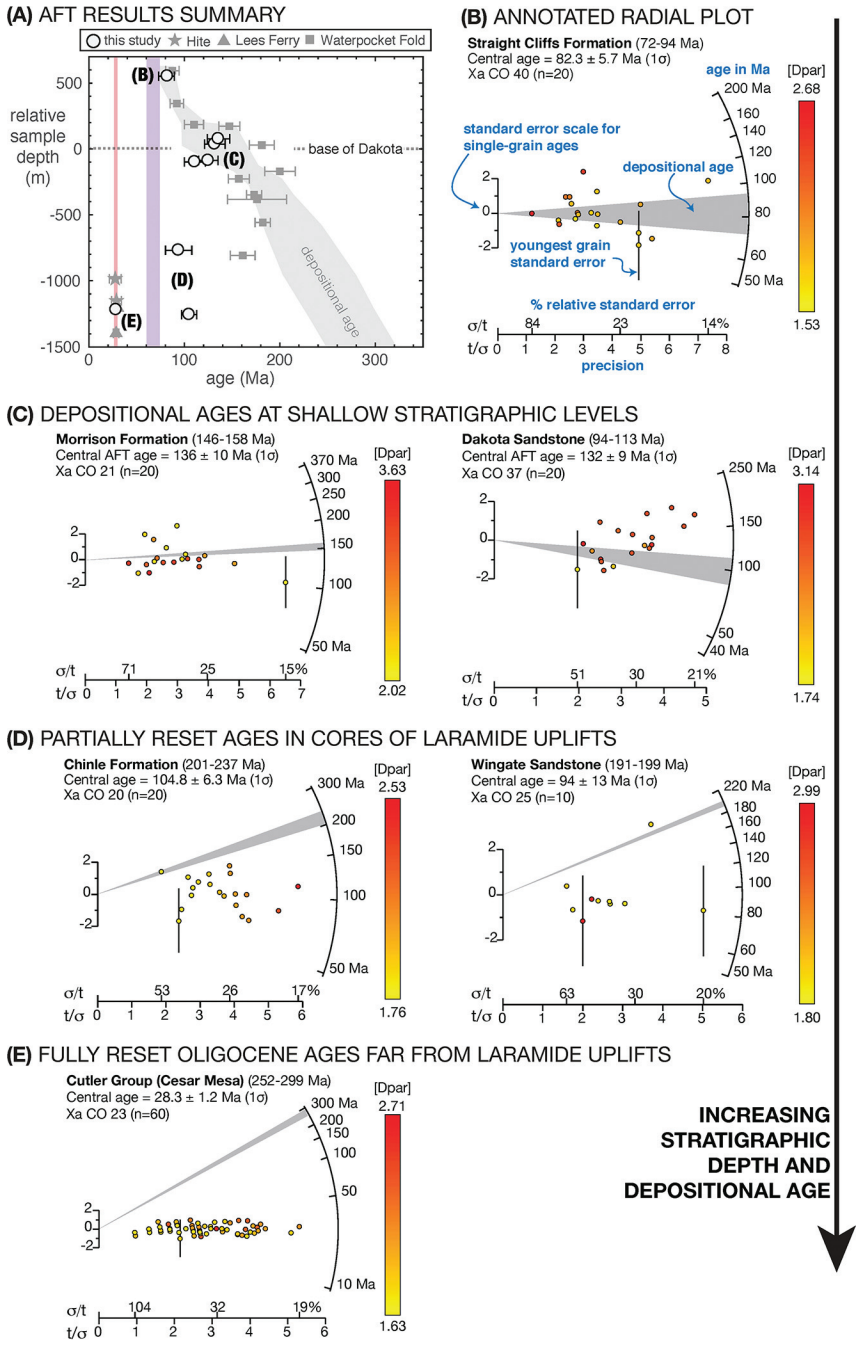

Fig. 6. AFT results from this and previous studies. (A) AFT central age (±1σ) vs. stratigraphic position relative to the base of the Dakota Sandstone as projected by Bump and Davis (2003). Pink and purple lines indicate the timing of Oligocene magmatism in the laccolith complexes and regional Laramide deformation, respectively, as in figure 3C. High in the stratigraphic section, AFT ages become older with depth, following the depositional age of the sampled unit. Below the Dakota Sandstone, AFT ages become younger with depth and are (partially) reset from their host sandstone depositional age. (B-D) Radial plots of AFT single-grain age data from samples from three categories of results. 2σ error bar shown on the youngest grain(s) to evaluate whether any grains are significantly younger than the stratigraphic age (gray line).

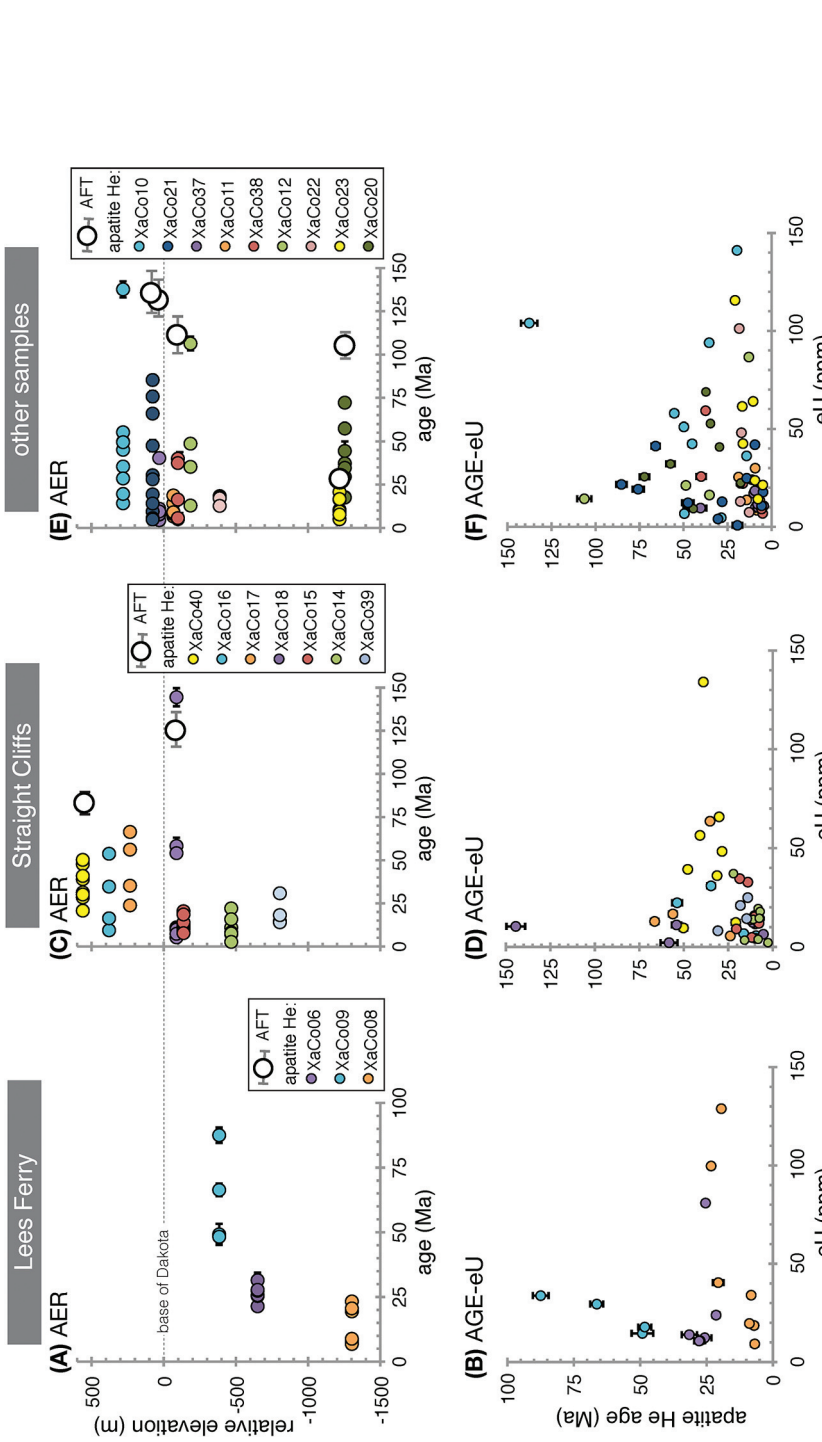

Fig. 7. AFT central ages and single-grain apatite He results from samples of the Lees Ferry to Hite transect, plotted against sample elevation relative to the base of the Dakota Sandstone (top panels) and apatite [eU] (bottom panels) to evaluate the sources of age dispersion. (A, B) A vertical profile up the Vermilion Cliffs above Marble Canyon near Lees Ferry. (C, D) A second vertical transect higher in the stratigraphic section from the Straight Cliffs of the Kaiparowits plateau. (E, F) Other samples.

wedge-shaped age-[eU] trend, with high-[eU] grains (>50 ppm) that all have ages of 40 to 30 Ma and low-[eU] grains that are as old at 50 Ma or young as 20 Ma (fig. 7D). This He age variability in low-[eU] apatite grains is typical of the entire dataset. A sample from the Jurassic Morrison Formation is an extreme example, with a mixed AFT central age of 125 ± 10 Ma (±1σ) and low-[eU] grains that range in He age from 144 to 5.2 Ma (XaCo18; figs. 7C and 7D). The three lowest-elevation samples from the Straight Cliffs have He ages of 30 to 3 Ma (figs. 7C and 7D).

Other samples.—The inter- and intra-sample apatite He age variability in the rest of the dataset (nine samples) is similar to results from the Straight Cliffs. All samples have at least one single-grain He age younger than 25 Ma (fig. 7E). Some samples have negative-slope age trends with substantial age variability at low [eU] (XaCo12, fig. 7F); others have positive-slope trends over a large range of [eU] with ages ~5 Ma at low [eU] values and ~20 to 16 Ma at [eU] values of 50 to 115 ppm (XaCo23). One sample, XaCo22 from the Henry Mountains region, has reproducible apatite He ages of 13 to 18 Ma. As with results from the Straight Cliffs, positive- and negative-slope age-[eU] trends coexist in individual sample results (for example, XaCo10, XaCo20) and make a wedge-shaped apatite He age-[eU] trend with substantial age variability at low [eU] (fig. 7F).

Identifying Samples for Thermal History Analysis

Only four samples from this study have apatite He ages on individual single-grain aliquots with <20 % 1σ standard deviation on the sample mean age: Moenave Formation sample XaCo06 from Lees Ferry, Entrada Sandstone sample XaCo22 from the Henry Mountains region near Mt. Ellsworth, Dakota Formation sample 12ABA07 from the Abajo Mountains, and Prospect laccolith igneous sample 12ABA05 from the Abajo Mountains. Igneous samples from the Abajo Mountains have very low-[eU] (mostly <20 ppm) apatite grains that exhibit substantial age variability, so despite sample 12ABA05 passing the standard deviation test, we chose not to rely on it for thermal history analysis because of the likelihood of ^{4}He implantation (Murray and others, 2014). Otherwise, the reproducible samples are useful for thermal history interpretations.

The considerable intra-sample He age dispersion in the remaining 32 samples is consistent with multiple, perhaps coexisting, sources of age variability. Only two sources of He age dispersion—radiation damage accumulation and annealing (RDAA, Flowers and others, 2009; Gautheron and others, 2009) and grain size variability—are currently useful for quantitative thermal history interpretations (Flowers and Kelley, 2011). Qualitative evaluation of [eU] and grain size effects identified seven samples with age dispersion consistent with these useful sources of age variability and therefore appropriate for additional thermal history analysis.

Before presenting thermal history modeling results, we next discuss the apatite He age variability that dominates this dataset. Another large apatite He dataset from sandstones of the north-central Colorado Plateau (n~300, Hoffman, ms, 2009) has an identical age range and pattern (fig. 8A). Therefore, the observed variability appears to be a characteristic of this region's rocks.

DIAGNOSING APATITE He AGE VARIABILITY

Expected He Age Variability

Dispersed apatite He ages from the Colorado Plateau's Permian-Cretaceous sedimentary bedrock are to be expected because the detrital grains have diverse predepositional ages, cooling histories, and compositions and therefore exhibit diverse susceptibilities to partial resetting (Gautheron and others, 2013). Moreover, the sedimentary units sampled were likely buried to depths between ~1.5 to 3 km. This

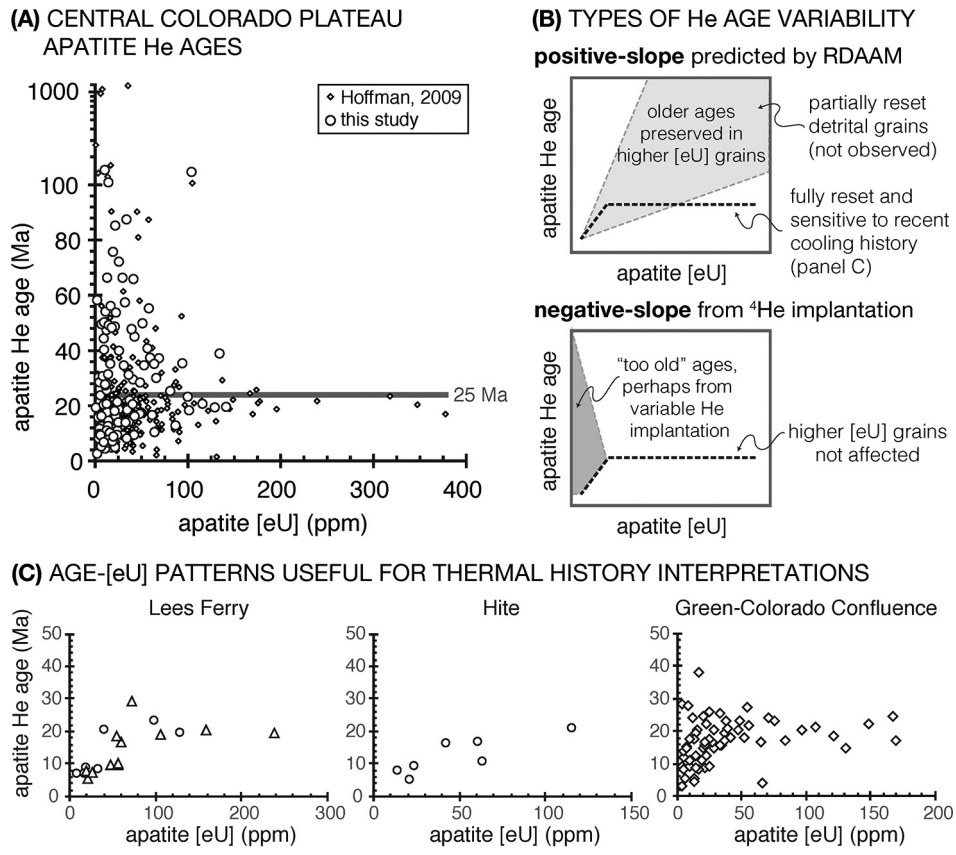

Fig. 8. Apatite grains from the central Colorado Plateau's Permian-Cretaceous sandstones have highly variable He ages (from this study and Hoffman, ms, 2009). These data form a distinctive wedge-shaped age-[eU] trend, with hundreds of percent age variability at [eU] < 50 ppm and a reproducible age of ~25 Ma in high-[eU] grains. (B) Types of apatite He age variability observed in this dataset include useful positive-slope age-[eU] trends (Flowers and others, 2008; Flowers and others, 2009) and negative-slope trends known to be produced by implantation of excess ^{4}He (Murray and others, 2014) and other parent nuclide zonation issues (for example, McKeon and others, 2013). The latter trends are identifiable but not useful for thermal history interpretations at this time. (C) A few samples from this and other studies (Hoffman, ms, 2009; Lee and others, 2013) have positive-slope patterns that provide rich thermal history information.

magnitude of burial, combined with typical geothermal gradients, is generally insufficient for complete resetting of the radiation damage and He content of apatite grains. Such partial resetting will have substantial effects on the temperature sensitivity of the apatite He system during subsequent rock cooling and is itself a function of a sample's thermal history (Fox and Shuster, 2014). We do not know enough about each grain's pre- and postdepositional history to specifically calculate these effects because a 5 to 10 °C difference in burial temperature has a substantial effect on the temperature sensitivity of the He system (Fox and Shuster, 2014). However, we can use the RDAAM to predict the expected pattern of age variability in rocks that have been at near-surface temperatures (<100 °C) for tens to hundreds of My: an age-[eU] trend where He age and grain [eU] are positively correlated (fig. 8b; Shuster and others, 2006; Flowers and others, 2007; Flowers and others, 2009). As a whole, the apatite He data from the central Colorado Plateau sandstones are dominated by the opposite trend—a negative-slope age-[eU] trend

(fig. 8A). This trend is inconsistent with the RDAA model because the oldest measured He ages are from the low-[eU] apatite grains, not the high-[eU] grains (fig. 8B). This pattern suggests that other sources of apatite He age variability dominate the He ages from sandstones of the central Colorado Plateau, co-mingling with and largely obscuring the RDAA signal that would perhaps otherwise characterize apatite He ages from across the region (fig. 8C).

Speculative Sources of He Age Variability Unrelated to Rock Thermal Histories

Although it is beyond the scope of this study to definitively diagnose the more insidious age dispersion in this dataset, we offer a brief summary of its potential causes. Intragranular zonation of [eU] (Ault and Flowers, 2012; McKeon and others, 2013) and neighboring [eU]-bearing phases (Spiegel and others, 2009; Gautheron and others, 2012; Murray and others, 2014) are known sources of apatite He age-[eU] trends with negative slopes and highly variable He ages in low-[eU] apatite grains. Intracrystalline zonation is unlikely to cause apatite He age dispersion of more that ~15 percent (Farley and others, 2011; Ault and Flowers, 2012; Gautheron and others, 2012; Johnstone and others, 2013). In central Colorado Plateau datasets, however, single-grain apatite He ages from single samples can vary by more than 100 Ma (>1000 % variability) in grains with <20 ppm [eU]. The only documented source of apatite He age variability of this magnitude is [eU]-rich mineral phases located outside the apatite grain that implant "excess" (that is, parentless) ^{4}He (Spiegel and others, 2009; Gautheron and others, 2012; Murray and others, 2014). The most extreme effects are from [eU]-rich GBPs (Murray and others, 2014). The He age variability that results from the effects of extragranular [eU] cannot be used for thermal history interpretations because full reconstruction of the *in situ* neighborhood of each dated apatite grain is not possible. We can, however, identify samples likely affected by He implantation using this diagnostic negative age-[eU] trend—a trend distinct from the positive-slope age-[eU] pattern characteristic of the useful RDAA effects (fig. 8B).

Along the Lees Ferry to Hite transect, there may be some geologic control on He age patterns. Negative-slope (He implantation) or positive-slope (RDAA) age-[eU] pattern trends appear to be dependent on sample stratigraphic and structural position (fig. 3, fig. 7). Sandstone samples with useful positive-slope trends are confined to the Triassic and deeper parts of the central Colorado Plateau stratigraphy. This could be because these rocks were buried to sufficient depth and temperature during the Cenozoic to reset predepositional age variability. Alternatively, or in addition, their stratigraphic position may have shielded these rocks from near-surface oxidized fluids capable of precipitating [eU]-rich GBPs. Such shielding could be caused by impermeable shale units, such was the Chinle or Moenkopi Formations, or perhaps the near-surface fluid flow had a finite penetration depth. Cenozoic fluid flow capable of mobilizing U has been documented by regional bleaching of the Navajo Sandstone and widespread digenetic oxides hosted in the Mesozoic sandstones of the Colorado Plateau (Reiners and others, 2014 and references therein).

A Triassic sandstone sample with a negative-slope He age-[eU] trend that ostensibly contradicts this idea (XaCo20, fig. 7E) may actually be consistent with it, because this sample is from the crest of the Circle Cliffs uplift (fig. 3). This structural position, in the exhumed core of a Laramide anticline, makes the Cenozoic history of this sample distinct from the other Triassic rocks sampled in this study, for two reasons. First, fold-related fracturing may have formed pathways for near-surface eU-mobilizing fluids to penetrate deeper in the stratigraphy; such fracturing is thought to control bleaching of the Triassic-Jurassic Glen Canyon Group rocks by the migration of petroleum-related fluids (Beitler and others, 2003). Second, AFT results from the steep limb of this anticline, the Waterpocket fold, suggest that the core of this structure may have exhumed as a local erosional response to Laramide deformation (Dumitru and others,

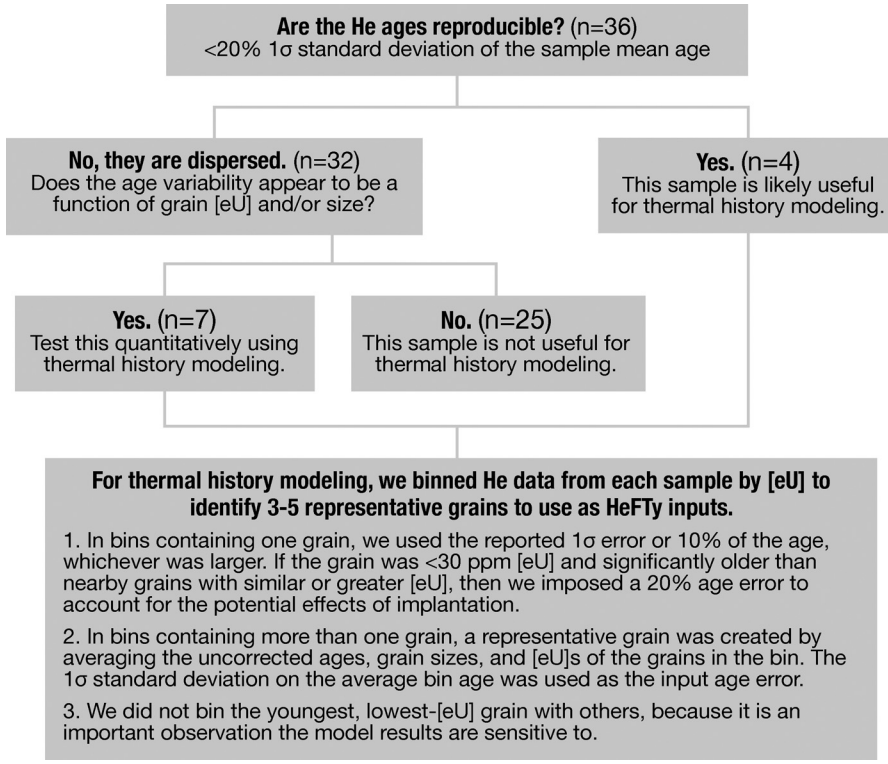

Fig. 9. Flowchart illustrating the approach used to evaluate the suitability of apatite He ages for thermal history modeling in this study.

1994). Thus, by early Cenozoic time these Triassic and older rocks could have been closer to the surface and near-surface fluids. Additionally, Laramide erosion could have removed shale units that would have otherwise acted as barriers to fluid flow.

In the laccolith-cored mountain ranges, the distribution of negative-slope and positive-slope He age-[eU] patterns is less systematic with respect to sample stratigraphic position than in other areas. We speculate that the magmatism *ca.* 28 to 25 Ma disrupted the regional fluid flow and/or distribution of GBPs. GBPs are abundant in the Henry Mountains intrusive complex (Murray and others, 2014), and we observe similar age patterns and GBP precipitates on grains in mineral separates from the La Sal and Abajo mountains porphyries and sandstones. The magnitude of the intra-sample He age variability in these samples (at most ~300 %) is less than that in sandstone samples collected far from the intrusive centers.

THERMAL HISTORY MODELING

Apatite He results from only ten sandstone samples are appropriate for thermal history modeling because they have reproducible apatite He ages or positive-slope He age-[eU] trends (figs. 8C and 9). We used the RDAAM in HeFTy (Ketcham, 2005; Flowers and others, 2009) to model each sample individually. We used HeFTy's inversion mode to predict cooling ages from hundreds of thousands of *tT* paths until either 100 good-fit paths were found or one million paths were attempted. Paths with acceptable fits ($0.05 <$ goodness of fit (GOF) < 0.5) are *not ruled out* by the cooling age data, and those with good fits (GOF > 0.5) are *supported* by the data (Ketcham, 2005).

For each model, we applied the following geologic constraints: (a) depositional temperature of 15 ± 5 °C, (b) range of burial temperatures at *ca.* 85 to 80 Ma calculated using the locally preserved thickness of Mesozoic stratigraphy and a 20 to 30 °C/km geothermal gradient, (c) one large constraint box to allow *tT* paths to explore temperatures from 0 °C to 160 °C and nonmonotonic histories during Cenozoic time, and (d) the modern surface temperature ± 2.5 °C. The apatite He results were binned to create inputs for HeFTy as described in figure 9. See Appendix and supplementary tables for detailed descriptions of the thermal history model setup and assumptions as suggested by Flowers and others (2015).

Laccolith-cored Mountain Ranges

Abajo Mountains.—In the Johnson Creek dome, the *ca.* 28 Ma Prospect laccolith intrudes the Permian Cutler Group in close proximity to samples 12ABA13 and 12ABA14. Therefore, in addition to the geologic constraints described above, we added three constraint boxes between 29 to 25 Ma to explore, but not require, a heating event at this time. These samples have positive-slope age-[eU] variability with single-grain He ages from 30 Ma and 11 Ma over a wide range of [eU] (table 1). Sample 12ABA13 has one anomalously old He age (43 Ma) in a low-[eU] grain (11 ppm), which we exclude from our analysis because of likely implantation effects (Murray and others, 2014). Modeling results of apatite He ages from both of these samples (figs. 10A and 10B) do not rule out Neogene cooling to <40 °C starting in middle Miocene time. More than 90 percent of the good-fit *tT* paths support that these samples were warmer than 40 °C, sitting at apatite He partial-retention temperatures, until at least 6 Ma. These samples are from the most deeply exhumed strata in the Abajo Mountains.

A sample with reproducible He ages (12ABA07, 15-21 Ma, table 1) from the Upper Cretaceous Dakota Sandstone sampled along Shay Ridge supports a wider range of Neogene *tT* histories (fig. 10C). Good-fit *tT* paths are all colder than 50 °C by *ca.* 8 Ma and only 12 percent are warmer than 40 °C at 6 Ma.

Sample 12ABA14 (fig. 10B) has an AFT age of 46.5 ± 4.2 Ma (±1σ) with long track lengths (14.46 ± 0.14, n=59) that, if included in the thermal history model, results in an inversion with no good- or acceptable-fit *tT* paths after 100,000 attempts. This result is the same with or without the additional *ca.* 29 to 25 Ma thermal history constraint boxes. The inflexible "frequentist" statistics used by HeFTy to judge fit may be responsible, as the RDAA and annealing models are not perfect predictors (Vermeesch and Tian, 2014). Additionally, AFT age and track lengths have a threshold-like behavior in HeFTy that make them acutely sensitive to reheating events like the one likely experienced by these rocks during Oligocene magmatism. A systematic forward-model approach using HeFTy (fig. A1) reveals this behavior and suggests a very narrow range of thermal histories, with a peak Oligocene T of ~135 °C, may fit the apatite He and AFT data from this sample. Given that our current understanding of damage annealing kinetics is limited (Fox and Shuster, 2014; Fox and others, 2017) and unlikely to accurately predict such a narrow range of peak T, we prefer the He-only inversion modeling results from this sample.

La Sal Mountains.—Two sandstone samples from the La Sal Mountains have Oligocene AFT ages (table 2) and dispersed apatite He ages with apparent age-[eU] trends. These samples were not collected in close proximity to mapped laccolith rocks, so we do not use extra constraint boxes as in the Abajo Mountains. Our approach to setting up thermal history models (Appendix, fig. 9) yields very few acceptable- and no good-fit *tT* paths (figs. 10D and 10E) after one million attempted paths for each sample. The acceptable-fit paths require similar *ca.* 30 Ma to recent thermal histories as the other thermal history modeling results presented here (figs. 10, 11, and 12) but do not support more specific Neogene thermal histories.

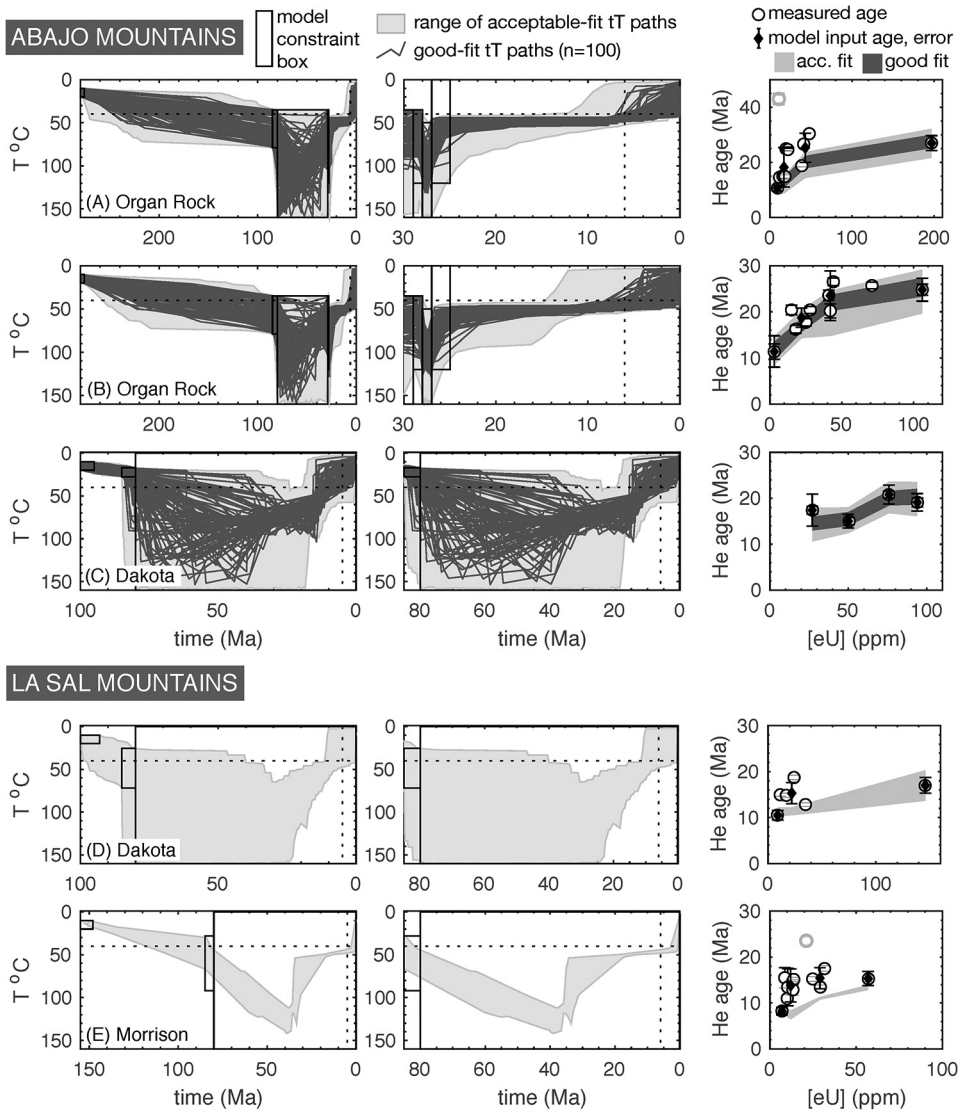

Fig. 10. Thermal history modeling results for samples from the laccolith-cored mountain ranges. In left and center time vs. temperature panels, black boxes are thermal history constraints, the light gray field contains all acceptable *tT* paths, and each dark gray line is a good-fit *tT* path. Dotted lines are 40 °C and 6 Ma reference lines. In He age vs. [eU] plots, white-filled circles are single-grain apatite He ages, black diamonds are single apatite grains and uncertainties input into the model, light gray circles are analyses excluded from modeling, and the gray fields encompass the age-[eU] trends for the acceptable- and good-fit *tT* paths. (A) 12ABA13. (B) 12ABA14. (C) 12ABA07 (D) 10SAL02. (E) 10SAL03. See text and Appendix for modeling details.

Canyonlands Transect

Vermilion Cliffs vertical profile near Lees Ferry.—Three samples collected in a vertical profile in the Vermilion Cliffs (fig. 7A) have reproducible or variable He ages (figs. 11A, 11B, and 11C) appropriate for thermal history modeling.

The lowest-elevation sample XaCo08 (fig. 11C, 1073 m) is from the Lower Triassic Moenave Formation, which is the oldest part of the stratigraphy we sampled in this

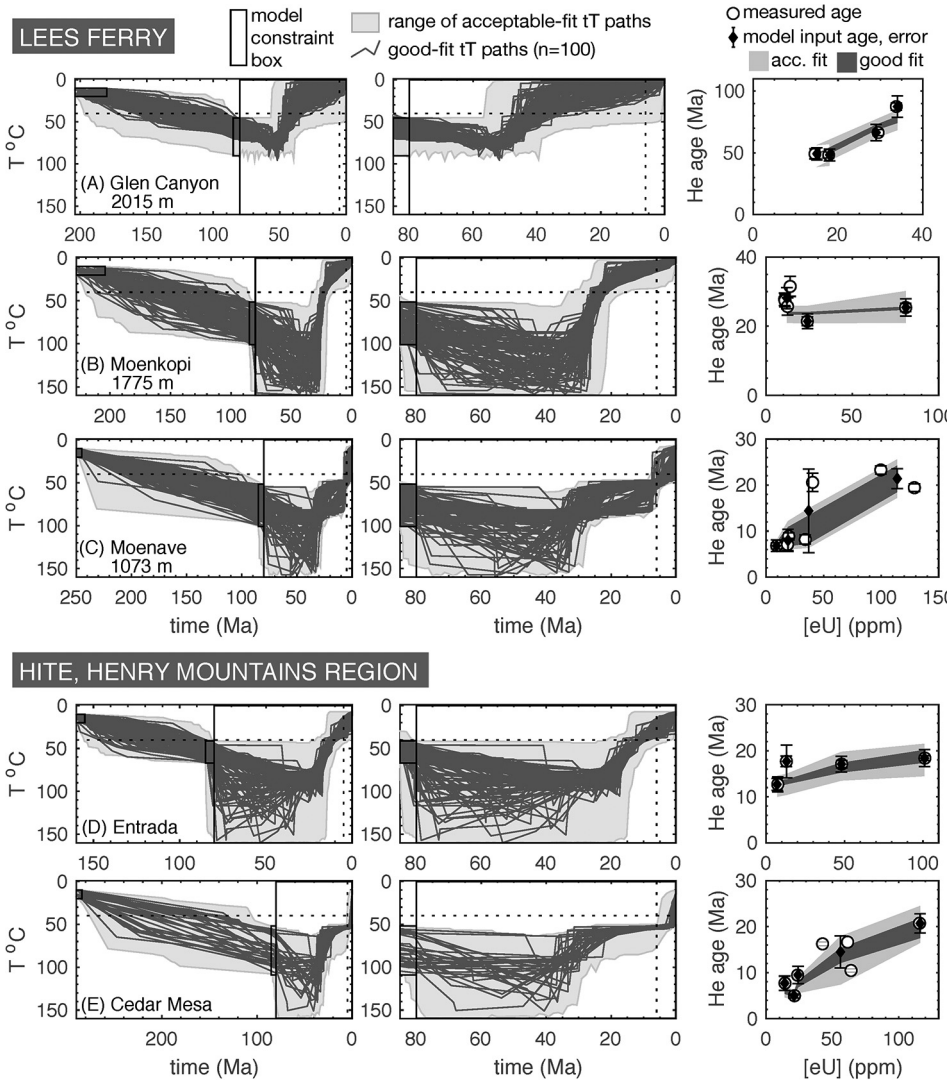

Fig. 11. Thermal history modeling results for sandstone samples from the Lees Ferry vertical profile and two samples from the Henry Mountains region. Dotted lines are 40 °C and 6 Ma reference lines. (A) XaCo09. (B) XaCo06. (C) XaCo08. (D) XaCo22. (E) XaCo23. See text and Appendix for modeling details.

location. This sample has dispersed apatite He ages, with single-grain ages as young as 6 Ma and the same positive-slope age-[eU] trend previously reported in the Permian rocks (~100 m lower) at river level (Lee and others, 2013). Published AFT data exist for nearby river-level samples from Marble Canyon (Kelley and Karlstrom, 2012), and we incorporate the AFT central age (28.4 ± 2.9 Ma) and track density data from sample 01GC92 into our thermal history model. The model results (fig. 11C) support a wide range of Paleogene thermal histories but by *ca.* 30 Ma require that this sample was at temperatures between 50 °C and 100 °C. This sample resided at those temperatures until the latest Miocene. Ninety-three percent of the good-fit *tT* paths are warmer than 45 °C until at least 6 Ma, and acceptable-fit paths rule out rock cooling <40 °C until after 8 Ma. This result agrees with the findings of Lee and others (2013).

Sample XaCo06 is from the Moenkopi Formation, which is ~700 m higher in the stratigraphy, and has reproducible He ages of 26 ± 3.3 Ma (table 1). The thermal history modeling results require sample cooling to <40 °C by *ca.* 20 Ma (fig. 11B). The model results support a wide range of Paleogene thermal histories but rule out temperatures colder than 50 °C prior to *ca.* 35 Ma.

Sample XaCo09 is from the Lower Jurassic Kayenta Formation of the Glen Canyon Group sampled at the top of the Vermilion Cliffs. This sample has low-[eU] grains (15–35 ppm) with dispersed He ages (44–88 Ma) that form a positive-slope age-[eU] trend. Thermal history modeling of this sample supports the hypothesis that this age variability is consistent with the effects of RDAA (fig. 11A). Model results require sample cooling to temperatures <40 °C after *ca.* 55 Ma, and good-fit *tT* paths support cooling between *ca.* 48 Ma and 27 Ma.

The modeling results agree with the age-elevation relationship between these samples (fig. 7A). This agreement confirms that the shallowest sample cooled earliest, perhaps during the Laramide-age erosion previously inferred from AFT ages in Marble Canyon (Kelley and Karlstrom, 2012), and was therefore not sensitive to the later Cenozoic history of the rocks exposed at Vermilion Cliffs. The middle-elevation sample clearly documents a period of rapid cooling during Oligocene time. Finally, the most deeply exhumed sample is most sensitive to the middle and late Cenozoic thermal history, supporting rock cooling during both Oligocene and Pliocene-Pleistocene time.

Henry Mountains region.—Sample XaCo23 is from the Permian Cutler Group on the shores of Lake Powell near Hite, Utah, approximately 20 km from outcrops of the Oligocene laccoliths. It has dispersed ages with a positive-slope age-eU trend, He ages from 5 Ma to 21 Ma, and an AFT central age of 28.4 ± 1.7 Ma (±1σ). The model results support a range of Paleogene thermal histories with temperatures >55 °C until the end of the Oligocene (fig. 11E). The good-fit *tT* paths (n=31) support a specific Neogene thermal history: temperatures warmer than 50 °C but colder than ~65 °C until after *ca.* 2.6 Ma. The acceptable-fit paths rule out the onset of this final pulse of cooling prior to 6 Ma. This result agrees with previous findings in the Henry Mountains near Mt. Hillers (Murray and others, 2016).

Sample XaCo22 from the Upper Jurassic Entrada Sandstone has reproducible apatite He ages of 16 ± 2.6 Ma. This sample was collected several kilometers from outcrops of the Mt. Ellsworth laccolith. The rock thermal histories supported by the good-fit paths narrow during Oligocene time (fig. 11D). The model results support rock cooling below 40 °C no earlier than *ca.* 16 Ma and cooling below 35 °C as recently as *ca.* 2.8 Ma.

Green-Colorado confluence.—Three samples collected from Permian and Triassic sandstones in Canyonlands near the confluence of the Green and Colorado rivers and dated by Hoffman (ms, 2009) have positive-slope apatite He age-[eU] trends that have not been previously modeled using the RDAAM. We modeled these data the same way as our own (fig. 12). One sample (fig. 12B) from the Triassic Moenkopi Formation yielded only 8 good-fit *tT* paths, and the results do not rule out thermal histories supported by the other samples. The good-fit *tT* paths for a sample from the Permian White Rim Sandstone (fig. 12C) support Oligocene rock cooling to temperatures between 45 °C and 80 °C by *ca.* 23 Ma followed by sample residence at partial-retention temperatures until at least 8 Ma. The model results from the Triassic Chinle Formation (fig. 12A) support a range of Paleogene thermal histories. The good-fit *tT* paths support sample residence at temperatures 70 to 45 °C through Miocene time, and 90 percent of these paths do not cool below 35 °C until after 6 Ma.

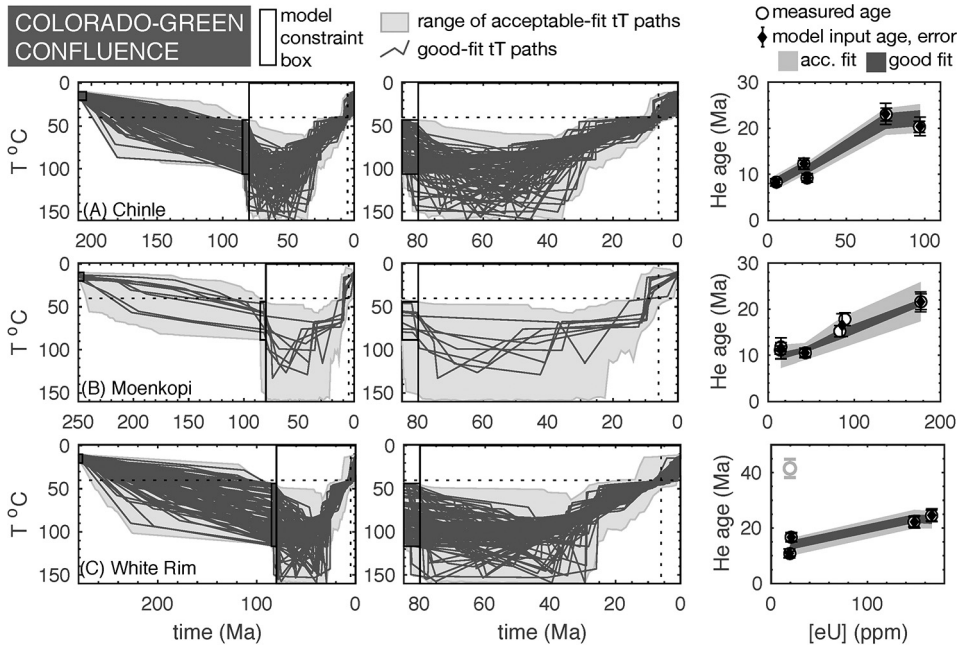

Fig. 12. Thermal history modeling results for sandstone samples from the Canyonlands region collected and dated by Hoffman (ms, 2009). Dotted lines are 40 °C and 6 Ma reference lines. (A) 07CP58. (B) 07CP72. (C) 08CP71. See text and Appendix for modeling details.

DISCUSSION

Samples from Canyonlands that are useful for thermal history analysis document different parts of the region's Cenozoic history depending on the temperatures at which they resided during the last *ca.* 80 My. Samples from relatively shallow stratigraphic levels and/or proximal to the hinges of Laramide anticlines (for example, Lees Ferry sample XaCo09, fig. 11A) cooled during Paleogene time and are therefore not sensitive to the Neogene history of the region. In contrast, samples from the deeply and recently exhumed regions (for example, the Johnson Creek dome in the Abajo Mountains, figs. 10A and 10B) resided for tens of millions of years at temperatures within the apatite He and AFT partial-retention/annealing zones and therefore document more recent, multiphase thermal histories. The richest thermal history information is contained in samples with positive-slope He age-eU patterns and Oligocene-Pliocene He ages because the coevolution of radiation damage and He diffusivity in apatite requires specific *tT* conditions. These samples must have spent significant time at partial-retention temperatures (45–60 °C) during Miocene time. The vertical profile at Lees Ferry (fig. 7A) encapsulates the resulting inter- and intra-sample age variability and thermal history sensitivity (figs. 11A, 11B, 11C). The AFT age vs. stratigraphic depth relationship (fig. 6A) we document across the Canyonlands region offers a complementary regional perspective on the cooling age architecture that likely characterizes this region.

The thermochronologic samples in this study that contain the richest thermal history information have positive-slope age-[eU] trends that document two periods of rock cooling: one starting no earlier than latest Miocene time *ca.* 6 Ma and the other during middle Cenozoic time *ca.* 30 to 20 Ma. This uniformity across the sample suite suggests that both the mountainous intrusive complexes and the deeply incised

Canyonlands of the Plateau interior share aspects of a common regional thermal history. Late and middle Cenozoic erosion events have been previously inferred from apatite thermochronology results in the Eastern Grand Canyon region (Flowers and others, 2008; Karlstrom and others, 2014), near Lees Ferry (Lee and others, 2013; Karlstrom and others, 2014), and along the southwestern Plateau margin (Karlstrom and others, 2017). We consider the candidate drivers of these two rock cooling events in the Canyonlands region separately, with a focus on how best to interpret the history of the Canyonlands region in middle Cenozoic time.

Late Cenozoic Rock Cooling

Central Colorado Plateau samples with positive-slope age-[eU] patterns and Oligocene-Pliocene single-grain He ages require a specific Neogene thermal history: residence at apatite He partial-retention temperatures (45–60 °C) throughout the Miocene followed by cooling to surface temperatures. This signal is present in Permian sandstones in the Abajo Mountains (this study); Triassic to Upper Jurassic sandstones in the Henry Mountains (Murray and others, 2016); Triassic (this study) and Permian rocks (Lee and others, 2013) at Marble Canyon; Permian rocks near Hite in Glen Canyon (this study); and Triassic and Permian sandstones along the Shafer Trail and Lathrop Canyon upstream of the confluence of the Green and Colorado rivers (Hoffman, ms, 2009 modeled in this study). Given the average modern geothermal gradient of 25 °C/km in this region (Blackett, 2004) and modern surface temperatures (which vary with sample location and elevation, see Appendix), we interpret this cooling as the erosion of ~1.5 km (± ~0.3 km) since the latest Miocene. There is substantial independent geologic evidence for kilometer-scale late Cenozoic erosion in the Canyonlands region (for example, Pederson and others, 2002; Cook and others, 2009; Darling and others, 2012; Karlstrom and others, 2012; Dorsey and Lazear, 2013; Lazear and others, 2013). The thermal history models of cooling ages from deeply exhumed samples in this study support that most of the ~1.5 km (± ~0.3 km) of erosion occurred rapidly during the last *ca.* 6 Ma, which is a useful refinement of previous estimates from the region (10–6 Ma, Hoffman and others, 2011; Karlstrom and others, 2012).

A rapid pulse of rock cooling due to erosion in the last ~6 Ma is likely a record of Colorado River base-level fall moving upstream as a wave of incision from the Grand Canyon region after river integration, although we do not resolve a clear spatial pattern of erosion onset in this dataset. This erosion event may also reflect isostatic feedback between erosion and uplift centered in the Glen Canyon region (Pederson and others, 2002; Lazear and others, 2013; Pederson and others, 2013). As in the Henry Mountains (Murray and others, 2016), at least a component of this exhumation in the Abajo Mountains is likely related to the response of this high-relief, high-elevation landscape to changes in global and regional climate in the last 3 to 2 Ma. Increased moisture, particularly snowpack, after 2.6 Ma may have accelerated rock cooling in this mountainous catchment by substantially enhancing the magnitude of bedrock erosion during spring runoff (Zhang and others, 2001; Pelletier, 2009; Johnson and others, 2010). Cool groundwater flowing downslope through these sandstones from the highest elevations (that is, Whipp and Ehlers, 2007) could also rapidly depress bedrock temperatures, though erosion is still required to bring these rocks from temperatures >40 °C to the surface.

The thickness of the Mesozoic stratigraphic section varies by up to ~2 km across the central Colorado Plateau, because the Cretaceous foreland basin deposits thicken substantially toward the Sevier orogenic front and the older massive aeolian sandstones generally thicken to the west (Hintze and Kowallis, 2009). Therefore, at each location where we infer ~1.5 km of late Cenozoic exhumation, we can evaluate whether some

earlier Paleogene erosion is also required, or if the entire thickness of the Mesozoic section was intact, at least locally, until the end of the Miocene.

Is Paleogene erosion of the central Colorado Plateau required?—In the La Sal and Abajo mountains there are abundant magmatic contacts between the Oligocene laccoliths and the Upper Cretaceous Mancos Shale, which requires that little Mesozoic sedimentary cover was removed prior to *ca.* 28 Ma (Hunt, 1958; Witkind, 1964). In the Abajo Mountains, the stratigraphy is sufficiently thin (Witkind, 1964; Hintze and Kowallis, 2009) that the entire Mesozoic section needed to be present in the Johnson Creek dome (~1200 m) through the Miocene to hold samples at ~40 to 50 °C, assuming a modern ~25 °C/km geothermal gradient and ~5 ± 2.5 °C surface temperature.

In contrast, the Triassic and older sandstones with interpretable cooling age trends far from the laccolith ranges do require Paleogene exhumation in order to be at apatite He partial-retention depths by early Miocene time, assuming a modern ~25 °C/km geothermal gradient: at least ~1 km in Marble Canyon near Lees Ferry; at least ~1 to 1.5 km in the Glen Canyon region near Hite; and at least 1 km at the confluence of the Green and Colorado rivers. Each of these locations is on the shallowly dipping flank of a Laramide fold ~35 to 50 km from the fold hinge. Resolving the timing and rate of this pre-Miocene rock exhumation—whether it is a middle Cenozoic erosion event, an earlier erosional response to Laramide shortening, or simply constant slow erosion (~20–30 m/My)—would help distinguish between proposed geodynamic drivers of Colorado Plateau surface uplift and erosion. Next, we demonstrate that available apatite thermochronology data cannot definitely resolve the region's pre-Neogene erosion history.

Middle Cenozoic Rock Cooling

In the thermal aureoles of the Oligocene intrusive complexes, middle Cenozoic rock cooling is likely the result of local postmagmatic thermal relaxation, whereas in sandstones from the canyons and mesas far (>20 km) from these intrusive complexes, this cooling is ambiguous and requires additional geologic information to interpret. This cooling could be documenting a period of rapid erosion, as inferred by previous thermochronologic studies in parts of the southwestern Plateau, Eastern Grand Canyon, Marble Canyon, and the Little Colorado River area (Flowers and others, 2008; Lee and others, 2013; Karlstrom and others, 2014; Karlstrom and others, 2017). Alternatively, we consider how thermal perturbations from mid-crustal magmatic systems are capable of resetting low-temperature thermochronometers in rocks sitting at partial-retention depths at the time of magmatism (Murray and others, 2018), and middle Cenozoic cooling could therefore reflect regional cooling of the upper crust following transient high heat flow driven by the magmatic flare-up in the region *ca.* 34 to 20 Ma (Coney and Reynolds, 1977; Dickinson and Snyder, 1978; Burke and McKee, 1979; Best and Christiansen, 1991). The laccoliths of the La Sal, Abajo, and Henry laccolith complexes, as well as the mid-crustal magma chambers that must have sourced them, are direct evidence of this crustal magmatism (Nelson and Davidson, 1993).

To investigate these end-member rock cooling scenarios, we use a 1D numerical conduction-advection model that tracks particle temperature and depth over time as a crustal thermal field responds to changing exhumation rates with or without the presence of a transient heat source at mid-crustal depths (see Appendix for model details). With this model, we predict the *tT* paths that rocks in the upper crust experience given various exhumation-only and magmatic-cooling scenarios (for example, fig. 13). We use *tT* paths computed by the model as forward-model inputs in HeFTy in order to predict the apatite He and AFT ages that would result, which can be compared to observed ages (fig. 14). These scenarios are not intended to capture best-fit solutions. Instead, they demonstrate that a range of reasonable Paleogene

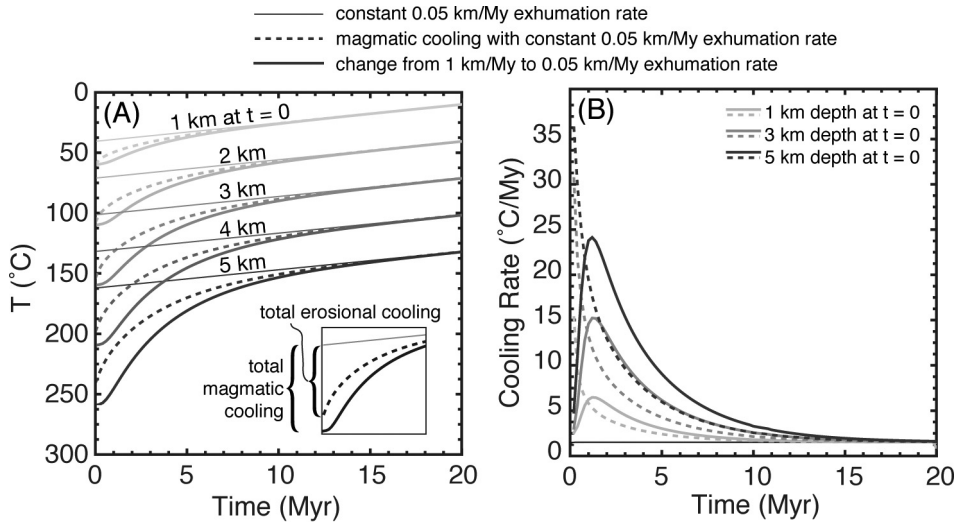

Fig. 13. Particle time-temperature paths and cooling rates calculated using a simple 1D finite-difference model (described in the Appendix). This model predicts, for example, (A) that a similar timescale and magnitude of rock cooling in the upper 5 km of the crust results from an instantaneous drop in exhumation rate from 1 to 0.05 km/Myr (dotted lines) and from the thermal relaxation of a 750 °C region at 15 km depth (solid lines) in a landscape steadily exhuming at 0.05 km/Myr. Both scenarios achieve equilibrium with the new state of the system in less than 10 Myr. (B) The cooling rates of these curves.

erosion histories are consistent with the observed apatite cooling ages if the geothermal gradient is considered a variable.

We implement a transient high heat-flow scenario in this model, with a peak geothermal gradient of ~50 °C/km, by holding mid-crustal (12–15 km) depths at temperatures of 610 to 760 °C for 5 My. This is consistent with (1) geophysical models (Condie and Selverstone, 1999) that suggest a density discontinuity at ~12 km in the Colorado Plateau lithosphere, which is a likely place for Oligocene magma to stall and pool while feeding the laccolith intrusive complexes and (2) ~300 °C of post-flare-up cooling in the lower crust suggested by an isotopic shift in volcanic rocks erupted across the Great Basin (Perry and others, 1993). Numerical results predict that rocks at partial-retention depths during the Oligocene equilibrate to the presence of this mid-crustal thermal anomaly within 1 to 2 My and that the postmagmatic thermal relaxation occurs in <10 My.

We compare model predictions of three possible histories of the Permian-Triassic rocks at Lees Ferry that result in Oligocene AFT ages and apatite He ages from 5 to 22 Ma that vary with eU (fig. 14A), as reported in this study and Lee and others (2013). Each modeled history has constant burial heating from *ca.* 250 Ma to 85 Ma followed by different Paleogene to early Miocene exhumation histories before final Pliocene-Pleistocene exhumation to the surface.

In the first scenario, only exhumation changes rock temperatures (fig. 14, solid line). The rock experiences a peak burial depth of 3.5 km (96 °C) at 85 Ma and then exhumes a total of ~0.5 km at a constant slow rate during the following 60 My. A period of rapid erosion (0.125 km/Myr) occurs from 25 to 15 Ma and exhumes the rock an additional 1.25 km to apatite He partial retention zone (PRZ) depths, where it resides until final rapid exhumation to the surface starting at 3 Ma (fig. 14B).

In the second and third scenarios (fig. 14, dashed and dotted lines), exhumation to apatite He PRZ depths occurs earlier in the Paleogene and the middle Cenozoic cooling

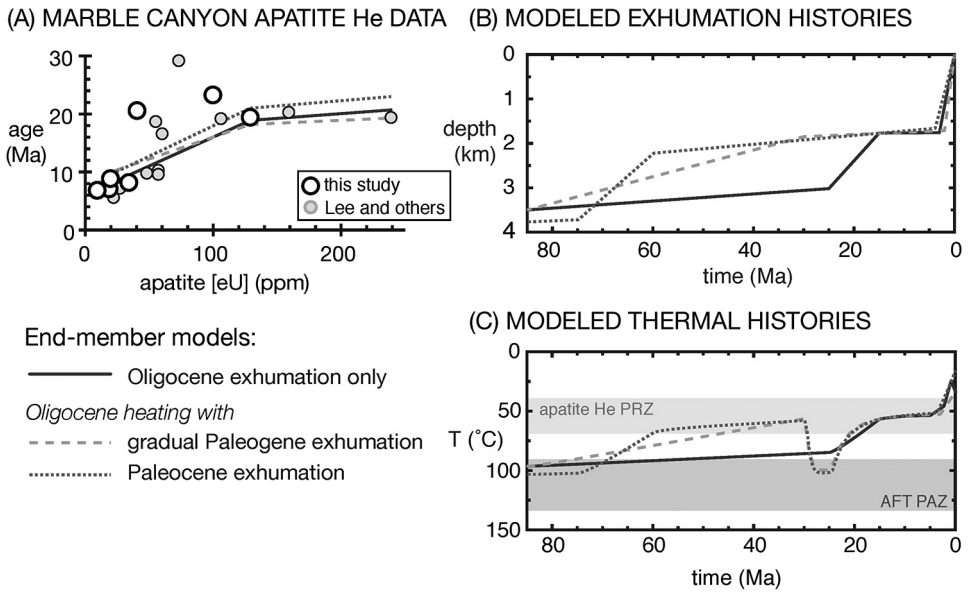

Fig. 14. Evaluation of erosion vs. thermal relaxation scenarios for the Colorado Plateau in middle Cenozoic time using samples from Lees Ferry and the 1D advection-conduction model. We compare three Paleogene erosion scenarios: solid line—rapid Oligocene erosion, which is the interpretation of rock cooling from previous studies; dashed line—gradual Paleogene erosion with Oligocene heating; dotted line—rapid Paleocene erosion with Oligocene heating. (A) Age-[eU] results from this study and Lee and others (2013). Ages that are older than the modeled trend are likely affected by He implantation (that is to say, fig. 8) and are therefore excluded from this exercise. (B) Sample depth vs. time. (C) Sample thermal histories were used as forward-model inputs in HeFTy in order to predict the resulting He age-[eU] pattern and AFT age (not shown). These three scenarios produce indistinguishable AFT ages and He age-[eU] trends; this modeling exercise is not intended to find a best-fit solution.

signal is the result of the transient thermal perturbation we impose between 30 and 25 Ma. In scenario two, the Triassic rock starts at the same depth and temperature at 85 Ma as scenario one but exhumes a total of 1.65 km between 85 and 30 Ma at a more rapid rate (0.03 m/Myr). At 30 Ma, the exhumation rate decreases to 0.005 m/Myr and is constant until 2 Ma, so the rock stays at ~1.8 km depth. However, the rock experiences a thermal perturbation during the Oligocene that heats it from ~56 °C at 30 Ma to a peak temperature of ~100 °C from 27 to 24.5 Ma. The rock cooling during postmagmatic thermal relaxation occurs at a similar rate as the rock cooling predicted by the middle Cenozoic exhumation (first) scenario (fig. 14C), so the predicted age-eU trends are indistinguishable (fig. 14A). Scenario three demonstrates that if we allow for an Oligocene thermal perturbation, the low-temperature thermochronologic data are insensitive to the pre-Oligocene exhumation history and, for example, the Triassic rock at Marble Canyon could have exhumed to apatite He PRZ depths by 60 Ma during a period of Laramide erosion at a rate of 0.1 m/Myr (fig. 14).

This modeling exercise suggests that, if geologically reasonable transient middle Cenozoic magmatic heating is allowed, the apatite cooling ages at Mable Canyon, Hite, and the Green-Colorado confluence support a range of erosion histories between two end-member scenarios. These include rapid erosion of ~1 km between 25 and 15 Ma, as previously proposed for Marble Canyon (Lee and others, 2013; Karlstrom and others, 2014) or ~1.5 to 2 km of earlier, possibly gradual, Paleogene erosion paired with a transient doubling of the geothermal gradient during middle Cenozoic time. Given this ambiguity, we propose that this middle Cenozoic rock cooling be referred to

as the *Middle Cenozoic Cooling Event*, the interpretation of which requires additional independent geologic evidence.

Canyonlands Erosion and Magmatism in Middle Cenozoic Time

Middle Cenozoic erosion.—Hunt (1956, 1969) first speculated about regional middle Cenozoic erosion across the Colorado Plateau *ca.* 38 to 26 Ma, suggesting that Dutton's (1882) "Great Denudation" of the Grand Canyon area was a regional, multiphase event. Apatite cooling ages from the southwestern Plateau, Eastern Grand Canyon, Marble Canyon (Naeser and others, 1989; Flowers and others, 2008; Kelley and Karlstrom, 2012; Lee and others, 2013), and the Little Colorado River (Karlstrom and others, 2017) reported by previous workers appear to support this idea. In turn, it has permeated many models of the Plateau's landscape evolution and uplift history (Flowers and others, 2008; Cather and others, 2012; Roberts and others, 2012; Lee and others, 2013; Sears, 2013; Karlstrom and others, 2014). There is direct evidence of middle Cenozoic erosion and aggradation in the southern Plateau region, as discussed below, as well as in the Uinta Mountains at the edge of the Plateau north of our study area (Hansen, 1986). However, no geologic observations require kilometer-scale Oligocene erosion of the Plateau interior in southeastern Utah.

Along the Mogollon Rim escarpment on the southwestern margin of the Plateau (fig. 15), thin Paleogene 'rim' gravels, canyons filled with Paleogene sediments, and angular unconformities between these deposits and Miocene volcanic rocks document a protracted and heterogeneous history of erosion and aggradation during the Laramide Orogeny though middle Cenozoic time (Peirce and others, 1979; Elston and Young, 1991; Holm, 2001). Elston and Young (1991) state that *ca.* 39 Ma AFT ages from the Eastern Grand Canyon (Naeser and others, 1989) suggest late Eocene tectonic uplift and erosion at the end of the Laramide triggered the end of rim gravel deposition. They note, however, that there is no direct evidence of this erosional event north of the Mogollon Rim. As Dumitru and others (1994) point out, the late Eocene (43–33 Ma) AFT ages in the Eastern Grand Canyon and Marble Canyon could be documenting rapid exhumation *ca.* 38 Ma or some more complicated, multiphase cooling history.

In the south-central Plateau, lower Oligocene aeolian sandstones in the Chuska Mountains and Mogollon-Datil volcanic field are interpreted as erosional remnants of a regionally extensive sand sea known as the Chuska Erg (fig. 15, Cather and others, 2008). Reconstruction of erg thickness and extent, together with several *ca.* 35 Ma paleosurfaces, prompted Cather and others (2008) to propose ~1200 m of Oligocene-Miocene erosion in the south-central Colorado Plateau region prior to the deposition of the Miocene Bidahochi Formation at *ca.* 16 Ma (fig. 15). Holm (2001) proposed a southwest to northeast sweep of erosion of the Triassic units in the same region during the Miocene. These interpretations are based on geologic evidence for middle Cenozoic aggradation and erosion in parts of the southwestern Plateau. However, no stratigraphic relationships or other geologic observations require a similar history several hundred kilometers to the north in our study area. In addition, there is no direct evidence of a middle Cenozoic paleoriver system and terminal basin capable of transporting and receiving the sediment that would have been generated by eroding ~1 km from the 100,000 km^2 area that comprises the extent of the Chuska Erg plus the Canyonlands region, although various models have been proposed (for example, Galloway and others, 2011; Sears, 2013).

Middle Cenozoic magmatism.—The magmatic record clearly documents that a prodigious amount of mantle-derived heat and melt was added to the Colorado Plateau region's lithosphere during the late Eocene and Oligocene. There is, however, little surficial expression of this event in the Canyonlands region. The lack of ignimbrite volcanism in the Plateau interior is attributed to several potential drivers. For example, the Farallon slab may have stayed shallow beneath the Plateau and

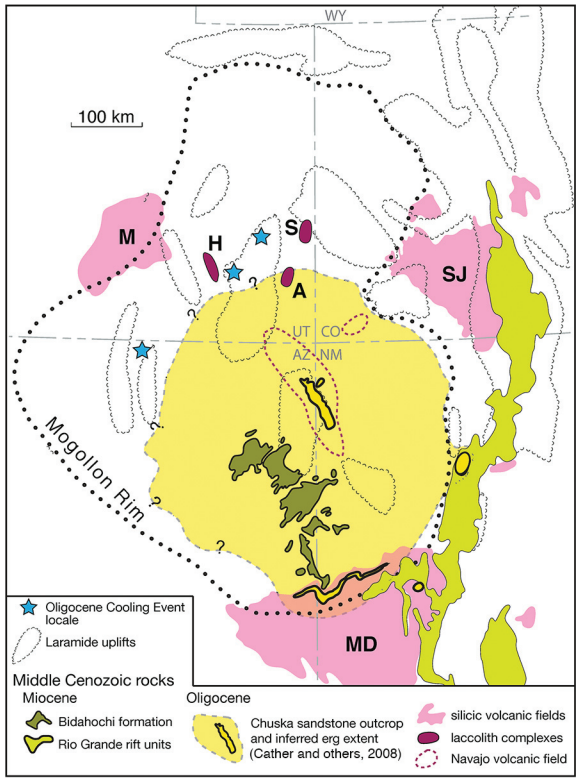

Fig. 15. Distribution of middle Cenozoic rocks of the Colorado Plateau modified from Cather and others (2008). Outline of the modern Colorado Plateau and state boundaries outlined by black and gray dotted lines, respectively. UT—Utah. CO—Colorado. NM—New Mexico. AZ—Arizona. WY—Wyoming. Volcanic fields: M—Marysvale, SJ—San Juan, MD—Mogollon-Datil. Navajo volcanic field extent from Semken (2003).

shielded it from the prolonged incursion of hot asthenosphere that drove magmatism in the surrounding regions (Humphreys, 1995; Humphreys and others, 2003). Alternatively, the regional pattern of flare-up volcanism may reflect how the composition of the mantle lithosphere controlled the production and aggregation of primary melt (Farmer and others, 2008; Lake and Farmer, 2015). Mantle xenolith data suggest that in contrast to surrounding regions, the Colorado Plateau's lithospheric mantle is depleted (that is, not fertile for melting) and forms a thick thermal boundary layer between the crust and the asthenosphere (Lee and others, 2001) that may have impeded the transfer of heat and melt into the lithosphere. In each case, the nature of the Colorado Plateau lithosphere and the lack of ignimbrite volcanism appear to suggest that the Plateau experienced normal (25 °C/km) crustal temperatures in the middle Cenozoic. However, the magmatic flare-up's potential thermal effects on the upper crust of the Colorado Plateau cannot be dismissed because magma rapidly advects heat from the mantle to the crust and thereby overcomes the time- and length-scale limitations of conductively heating the lithosphere by increasing the basal heat flow alone (Murray and others, 2018).

Previous apatite thermochronology results from the eastern Colorado Plateau and the neighboring Rio Grande rift, southern Rocky Mountains, and southern High Plains has prompted occasional discussion of the middle Cenozoic as a time of high

heat flow (Leonard and others, 2002; House and others, 2003; Roy and others, 2004; Ricketts and others, 2016; Landman and others, 2016; Rønnevik and others, 2017). Samples from the Uncompahgre Plateau east of the La Sal Mountains experienced complete resetting during late Eocene to Oligocene time, which Rønnevik and others (2017) attributed to the magmatic flare-up. In the southern Rocky Mountains along the eastern and southeastern Plateau margin, Roy and others (2004) demonstrated that the voluminous magmatism in the San Juan and Mogollon-Datil volcanic fields had the capacity to generate *ca.* 25 Ma AFT ages in northern New Mexico and western Colorado, though Roy and others interpreted this as a regional signal of an erosional response to magmatism-driven uplift. In the Rio Grande rift (House and others, 2003) and parts of the Rocky Mountains and the southern High Plains (Leonard and others, 2002; Roy and others, 2004; Landman and others, 2016), an Oligocene thermal anomaly is documented by an abrupt vertical transition in AFT ages (that is, a paleoisotherm of ~110 °C) in which ages are *ca.* 30 to 25 Ma below this transition and >100 Ma above.

AFT ages from Canyonlands region have a similar vertical architecture of cooling ages (fig. 6) in the most deeply exhumed parts of the Colorado River corridor. In the Henry Mountains region, the Jurassic Morrison Formation ~10 km north of the intrusive complex has a Jurassic depositional AFT age and long track lengths (Murray and others, 2016), whereas neighboring Permian rocks from ~1 km deeper in the stratigraphic section have AFT ages of 25 to 27 Ma (this study; Huntoon and others, 1999). Therefore, between these two samples is the same abrupt age transition observed in eastern Colorado Plateau and Rocky Mountains. Samples from the Waterpocket fold ~20 km west of the Henry Mountains have entirely unreset or partially reset AFT ages older than 100 Ma with AFT length data suggest cooling during the Laramide (*ca.* 75 Ma) followed by moderate middle Cenozoic heating, perhaps due to the Henry Mountains intrusive complex to the east and Marysvale volcanic fields to the west (Dumitru and others, 1994).

Despite geologic evidence for extensive magmatic activity and the trends in the low-temperature thermochronologic data, a thermal relaxation mechanism for regionally extensive middle Cenozoic rock cooling has not been previously proposed for the Colorado Plateau itself or the Canyonlands region in particular.

The Middle Cenozoic Cooling Event.—Rock cooling documented by apatite He ages, AFT ages, and thermal history model results in the Canyonlands region, as with all thermochronologic results, requires interpretation in the context of independent geologic information. Unlike in the south-central and southwestern parts of the Colorado Plateau, there is no geologic evidence for middle Cenozoic erosion in our study area. Instead, the only Oligocene features are the Abajo, La Sal, and Henry mountains laccolith complexes, which reflect the unequivocal fact that the during Oligocene time, the Colorado Plateau region was sitting in the midst of one of the largest flare-ups of magmatic activity in the geologic record.

We have modeled our magmatic-cooling hypothesis of the *Middle Cenozoic Cooling Event* as a thermal anomaly in the middle crust. However, in reality, a warm middle Cenozoic geothermal gradient would have an upper crustal thermal field with a complex spatial and temporal pattern produced by a combination of (1) paleotopography, (2) minor far-field effects of the massive volcanic centers that surround the Plateau (fig. 15), (3) moderate effects from a warm lower crust, where mantle melts would pool and geophysical evidence of extensive mafic intrusions was recently reported in the southern Colorado Plateau (Tork Qashqai and others, 2016), and (4) the additive and more proximal effects of the upper crustal magma chambers including the laccolith complexes, which intruded at ~850 °C (Nelson and others, 1992). It is also possible that cooling to a normal (that is, 25 °C/km) geothermal gradient in early Miocene time could mark the end

of a much longer period of elevated crustal temperatures that started when magmatism moved through the region during Late Cretaceous time (Snyder and others, 1976; Erdman and others, 2016).

CONCLUSIONS

The importance of erosion in the history of the Colorado Plateau is obvious to even the casual observer. However, apatite thermochronologic results suggest that parts of this story, as viewed from the perspective of rock cooling ages and thermal histories, are challenging to untangle from heating and cooling related to the region's middle Cenozoic magmatic history. Additionally, interpreting the thermal histories of sandstones from the Colorado Plateau pushes the limits of our current ability to identify the mechanisms that control He mobility in each detrital apatite grain. Here, we follow a standard approach to dispersed apatite He datasets (Flowers and Kelley, 2011) and limit our thermal history analysis to samples with reproducible apatite He ages or He age dispersion that we can clearly attribute to the effects of grain size (Reiners and Farley, 2001) and the coevolution of radiation damage and He diffusivity in apatite (Shuster and others, 2006; Flowers and others, 2009; Gautheron and others, 2009).

Most thermochronologic samples from the Canyonlands region suffer from additional, currently intractable, He age dispersion in low-[eU] grains (figs. 8A, 8B). A distinctive pattern of age variability in apatite He age-[eU] trends (fig. 8A) appears to be characteristic of the sedimentary rocks of the Canyonlands region. Old and variable He ages in low-[eU] apatite grains, which manifest as negative-slope He age-[eU] trends (fig. 8B), are likely the result of ^{4}He implantation, perhaps from the U-Th-rich grain boundary phases that are common in this region (Murray and others, 2014). The abundance of this type of He age complexity appears to be related to stratigraphic position, so we tentatively propose that it reflects a history of diagenesis and fluid flow capable of mobilizing U and Th and variably affecting apatite He ages in the 1 to 2 km of stratigraphy above the uraniferous Triassic Chinle Formation.

Apatite cooling ages useful for thermal history modeling document different parts of the region's thermal history as a function of how a sample's stratigraphic position and location contributed to its residence time at fission-track partial-annealing and He partial-retention temperatures (for example, figs. 7A and 11). Our thermal history modeling of deeply exhumed rocks clearly documents ~1.5 km of erosion in the Canyonlands region since the latest Miocene. However, it is not yet possible to resolve the timing or rate of Paleogene erosion in the Canyonlands region using thermochronology due to likely thermal effects of the magmatic flare-up that swept across the region *ca.* 34 to 20 Ma. Given the current difficulty of distinguishing between magmatic and exhumational cooling using thermochronology alone (Murray and others, 2018) and our ability to fit apatite thermochronology data in this study with either driver of middle Cenozoic rock cooling (fig. 14), we propose that all middle Cenozoic rock cooling on the Colorado Plateau should be described as documenting a *Middle Cenozoic Cooling Event* of ambiguous origin(s). The likely drivers of middle Cenozoic rock cooling should be determined based on local evidence for erosion and/or magmatic activity.

Despite ambiguity regarding the timing and rate of Paleogene erosion in the Canyonlands region, its spatial pattern and magnitude are clear. At Lees Ferry, Hite, and the Green-Colorado confluence, ~1 to 1.5 km of Paleogene erosion is required to exhume samples to apatite He partial-retention depths by early Miocene time. In contrast, Paleogene erosion likely did not remove Mesozoic strata from the Abajo Mountains (this study) or the Henry Mountains (Murray and others, 2016); indeed, the entire Mesozoic stratigraphic section is still intact in multiple parts of the Plateau interior today (fig. 2). After Paleogene time, the Canyonlands region was largely isolated from erosion until after the development of the modern Colorado River system *ca.* 6 Ma.

ACKNOWLEDGMENTS

KEM acknowledges support from an NSF GRFP award, an ARCS Phoenix Chapter Prentice Scholarship, a GSA student research grant, and a P.E.O. Scholar Award. A summer scholarship from ConocoPhilips through UA Geosciences funded fieldwork. NSF-EAR 1338583 supports the Arizona LaserChron Center. XR was supported by a CIFAR Postdoctoral Fellowship. Thanks to Ryan Porter for discussions of geophysical evidence for mid-Cenozoic magmatism in the central Colorado Plateau region and to Jay Quade, George Davis, and Mihai Ducea for comments on early versions of the manuscript. We thank Matthew Dettinger and Jordan Holsapple for assistance in the field. Uttam Chowdhury, Erin Abel, and Nicky Geisler assisted in the lab. We acknowledge thorough and constructive reviews from Joel Pederson, Karl Karlstrom, one anonymous reviewer, and the editors at *American Journal of Science*.

APPENDIX

Analytical Methods

Zircon U/Pb.—We picked ~50 zircon grains from each igneous sample and mounted them on a 1-inch epoxy mount with Sri Lanka and Fish Canyon Tuff zircon standards. The mounts were sanded down to a depth of ~20 μm, polished, imaged, and cleaned. Prior to analysis, we imaged grains with a Hitachi 3400N SEM and a Gatan CL2 detector system in order to optimally locate analysis pits and assist in interpreting results. The isotopic analyses involved ablation of zircon with a Photon Machines Analyte G2 excimer laser equipped with HelEx ablation cell using a spot diameter of 20 μm. The ablated material was carried in He into the plasma source of the Element2 HR-ICP-MS, which sequences rapidly through U, Th, and Pb isotopes.

Apatite Fission Track.—Apatite grains were mounted in epoxy resin, alumina and diamond polished, and spontaneous fission tracks were revealed by etching with 5.5 M HNO_3 at 20 °C for 20 s. Samples were irradiated at the Oregon State University Triga Reactor, Corvallis, USA. The neutron fluence was monitored using European Institute for Reference Materials and Measurements (IRMM) uranium-dosed glasses IRMM 540R. After irradiation, induced tracks in the mica external detectors were revealed by etching with 48 % HF for 20 minutes. Spontaneous and induced FT densities were counted using an Olympus BX61 microscope at 1250× magnification with an automated Kinetek Stage system. Apatite FT lengths and Dpar values were measured using FTStage software, an attached drawing tube and a digitizing tablet supplied by T. Dumitru of Stanford University calibrated against a stage micrometer. According to the recommendations of Hurford (1990), an apatite IRMM 540R zeta calibration factor of 368.1±14.9 was obtained by repeated calibration against a number of internationally recognized age standards, including Durango and Fish Canyon apatite. For young ages with low track counts, a binomial (or Z) age was calculated with 95 % confidence intervals using the F-distribution method described by Galbraith (2005).

Apatite (U-Th-Sm)/He.—Individual apatite grains were wrapped in niobium foil packets and heated to ~1065 °C for 3 minutes using a Nd-YAG or diode laser in a laser cell attached to an ultrahigh vacuum gas extraction line. Extracted He gas was spiked with ^{3}He, purified using cryogenic and gettering methods, and analyzed on a quadrupole mass spectrometer. Analysis of a known quantity of ^{4}He was performed after every 4 to 5 unknown analyses to monitor instrumental sensitivity drift. Then, apatite grains were dissolved in HNO_3 at ~90 °C for 1 h. U, Th, and Sm contents of each grain were measured by isotope dilution and solution ICP-MS on an Element 2 ICP-MS, as described by Reiners and others (2004) and Reiners (2005), using ^{233}U-^{229}Th and ^{147}Sm spikes. After 2012, a ^{44}Ca spike was used to calculate the stoichiometric apatite mass and volume. Precision on measured U/Th values was typically better than 0.5 %.

Thermal (tT) History Modeling

The method used to determine the suitability of each sample for thermal history modeling and the selection of three to five representative apatite He analyses to use as model inputs is described in figure 9. Thermal history modeling was performed using HeFTy v. 1.9.3 (Ketcham, 2005). We used the following apatite He kinetic parameters: 'RDAAM (Flowers and others, 2009)'; precision 'good'; stopping distances 'Ketcham and others, 2011'; alpha calculation 'redistribution'; rmr0 '0.8'; and age alpha-correction 'Ketcham and others, 2011'. The statistical fitting criteria used were the HeFTy defaults: a merit value for 'good' fit of 0.5 and a merit value for 'acceptable' fit of 0.05. Thermal history models had four *tT* constraints as summarized in the main body text: sample deposition, sample burial *ca.* 85 to 80 Ma, a range of *tT* paths during the Cenozoic, and the modern surface temperature projected to the sample elevation using a temperature lapse rate of -6.5 °C/km (Minder and others, 2010). Apatite cooling ages of modeled samples postdate sample deposition by more than 100 My, but our simulations begin at a sample's depositional age in order to permit accumulation and annealing of radiation damage over a geologically relevant period. Burial

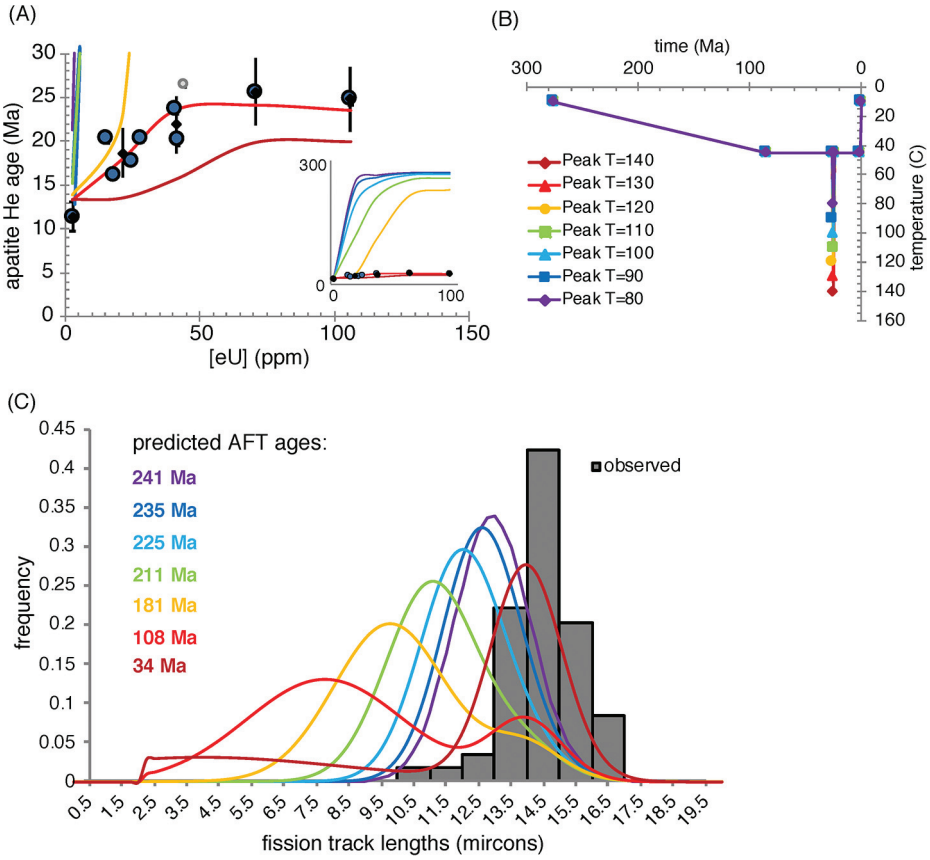

Fig. A1. Comparative results of forward models of apatite He and AFT data from sample 12ABA14, which do not yield acceptable or good-fit *tT* paths when jointly modeled after 100,000 *tT* path attempts. With the currently accepted kinetics implemented in HeFTy, these systems are very sensitive, perhaps unrealistically so, to the combination of Paleogene burial temperature and peak Oligocene heating temperatures likely experienced by this sample. (A) He age-[eU] plot with He ages from sample 12ABA14 and forward-modeled age-[eU] trends predicted from the time-temperature histories shown in (B). (C) Observed fission-track length distribution compared to those predicted by the same forward models. Peak Oligocene temperatures of ~137 °C would produce the observed track lengths, approximate AFT central age, and He age-[eU] trend.

depths *ca.* 85 to 80 Ma were calculated using the local stratigraphic thicknesses that are compiled across the region in Hintze and Kowallis (2009) and supplemented by local studies in the Abajo (Witkind, 1964) and Henry (Hunt and others, 1953) mountains.

We used *tT* path characteristics with random subsegment spacing. Paths between the *tT* constraints had the following characteristics: 2G, 1Ev, 2Ev. Models of two samples collected next to the Prospect laccolith in the Abajo Mountains (figs. 10A and 10B) included three additional 'laccolith' *tT* constraint boxes to explore, but not require, transient heating and cooling during the emplacement of the laccolith *ca.* 28 Ma. The *tT* paths between the constraints in these models had the following characteristics: 2G, 0E, 1Ev, 0E, 0E, 2E. For all thermal history models, the number of paths attempted was the number required to return 100 good-fit paths or one million paths. Models with the additional 'laccolith' constraints were also run for 100,000 attempts with four constraint boxes instead of seven (that is to say, run identically to all other models) to confirm that a significantly different result was not returned.

Supplementary tables (http://earth.geology.yale.edu/%7eajs/SupplementaryData/2019/Murray) include all additional information required to justify and reproduce the thermal history modeling results presented in this paper (Flowers and others, 2015). This includes the complete AFT (supplementary table 2) and

apatite He analyses (supplementary table 3) as well as the specific inputs and constraints used to model samples from the Abajo Mountains (supplementary table 4), La Sal Mountains (supplementary table 5), Lees Ferry (supplementary table 6), the Hite-Henry Mountains region (supplementary table 7), and near the Green-Colorado river confluence (supplementary table 8).

Thermal Modeling

Our 1D conduction-advection model tracks particle temperature and depth in a thermal field that evolves with time using a numerical finite-difference method. The code is written in MATLAB® and uses operator splitting, with advection solved by the upwind differencing method (without corrections) and conduction solved using the Crank-Nicolson method. Dirichdlet boundary conditions are $T_{surface}$ = 10 °C and T_{base} = 900 °C. The thermal diffusivity is 25 km^2/My. The model domain is 30 km thick, with a node spacing of 10 m. The model time step is 0.025 My. The stability of the advection solution is monitored using the Courant-Friedrichs-Lewy condition (that is, Courant Number), which must be less than 1.

REFERENCES CITED

Armstrong, R. L., 1969, K-Ar Dating of Laccolithic Centers of Colorado Plateau and Vicinity: GSA Bulletin, v. 80, n. 10, p. 2081–2086, https://doi.org/10.1130/0016-7606(1969)80[2081:KDOLCO]2.0.CO;2

——— 1974, Magmatism, orogenic timing, and orogenic diachronism in the Cordillera from Mexico to Canada: Nature, v. 247, n. 5440, p. 348–351, https://doi.org/10.1038/247348a0

Armstrong, R. L., and Ward, P., 1991, Evolving Geographic Patterns of Cenozoic Magmatism in the North American Cordillera: The Temporal and Spatial Association of Magmatism and Metamorphic Core Complexes: Journal of Geophysical Research-Solid Earth, v. 96, n. B8, p. 13201–13224, https://doi.org/10.1029/91JB00412

Ault, A. K., and Flowers, R. M., 2012, Is apatite U-Th zonation information necessary for accurate interpretation of apatite (U-Th)/He thermochronometry data?: Geochimica et Cosmochimica Acta, v. 79, n. C, p. 60–78, https://doi.org/10.1016/j.gca.2011.11.037

Beitler, B., Chan, M. A., and Parry, W. T., 2003, Bleaching of Jurassic Navajo Sandstone on Colorado Plateau Laramide highs: Evidence of exhumed hydrocarbon supergiants?: Geology, v. 31, n. 12, p. 1041–1044, https://doi.org/10.1130/G19794.1

Best, M. G., and Christiansen, E. H., 1991, Limited extension during peak Tertiary volcanism, Great Basin of Nevada and Utah: Journal of Geophysical Research-Solid Earth, v. 96, n. B8, p. 13509–13528, https://doi.org/10.1029/91JB00244

Best, M. G., Barr, D. L., Christiansen, E. H., Gromme, S., Deino, A. L., and Tingey, D. G., 2009, The Great Basin Altiplano during the middle Cenozoic ignimbrite flareup: Insights from volcanic rocks: International Geology Review, v. 51, n. 7–8, p. 589–633, https://doi.org/10.1080/00206810902867690

Best, M. G., Christiansen, E. H., de Silva, S. L., and Lipman, P. W., 2016, Slab-rollback ignimbrite flareups in the southern Great Basin and other Cenozoic American arcs: A distinct style of arc volcanism: Geosphere, v. 12, n. 4, p. 1097–1135, https://doi.org/10.1130/GES01285.1

Bird, P., 1979, Continental delamination and the Colorado Plateau: Journal of Geophysical Research-Solid Earth, v. 84, n. B13, p. 7561–7571, https://doi.org/10.1029/JB084iB13p07561

——— 1984, Laramide crustal thickening event in the Rocky Mountain Foreland and Great Plains: Tectonics, v. 3, n. 7, p. 741–758, https://doi.org/10.1029/TC003i007p00741

Blackett, R. E., 2004, Geothermal Gradient data for Utah: Utah Geological Survey, a division of Utah Department of Natural Resources, 49 p.

Bowring, S. A., and Karlstrom, K. E., 1990, Growth, stabilization, and reactivation of Proterozoic lithosphere in the southwestern United States: Geology, v. 18, n. 12 p. 1203–1206, https://doi.org/10.1130/0091-7613(1990)018<1203:GSAROP>2.3.CO;2

Braun, J., Robert, X., and Simon-Labric, T., 2013, Eroding Dynamic Topography: Geophysical Research Letters, v. 40, n. 8, p. 1494–1499, https://doi.org/10.1002/grl.50310

Bump, A. P., and Davis, G. H., 2003, Late Cretaceous–early Tertiary Laramide deformation of the northern Colorado Plateau, Utah and Colorado: Journal of Structural Geology, v. 25, n. 3, p. 421–440, https://doi.org/10.1016/S0191-8141(02)00033-0

Burke, D. B., and McKee, E. H., 1979, Mid-Cenozoic volcano-tectonic troughs in central Nevada: GSA Bulletin, v. 90, n. 2, p. 181–184, https://doi.org/10.1130/0016-7606(1979)90<181:MVTICN>2.0.CO;2

Bursztyn, N., Pederson, J. L., Tressler, C., Mackley, R. D., and Mitchell, K. J., 2015, Rock strength along a fluvial transect of the Colorado Plateau – quantifying a fundamental control on geomorphology: Earth and Planetary Science Letters, v. 429, n. C, p. 90–100, https://doi.org/10.1016/j.epsl.2015.07.042

Carroll, A. R., Chetel, L. M., and Smith, M. E., 2006, Feast to famine: Sediment supply control on Laramide basin fill: Geology, v. 34, n. 3, p. 197–4, https://doi.org/10.1130/G22148.1

Cassel, E. J., Graham, S. A., Chamberlain, C. P., and Henry, C. D., 2012, Early Cenozoic topography, morphology, and tectonics of the northern Sierra Nevada and western Basin and Range: Geosphere, v. 8, n. 2, p. 229–249, https://doi.org/10.1130/GES00671.1

Cather, S. M., Connell, S. D., Chamberlin, R. M., McIntosh, W. C., Jones, G. E., Potochnik, A. R., Lucas, S. G., and Johnson, P. S., 2008, The Chuska erg: Paleogeomorphic and paleoclimatic implications of an Oligocene sand sea on the Colorado Plateau: GSA Bulletin, v. 120, n. 1–2, p. 13–33, https://doi.org/10.1130/B26081.1

Cather, S. M., Chapin, C. E., and Kelley, S. A., 2012, Diachronous episodes of Cenozoic erosion in

southwestern North America and their relationship to surface uplift, paleoclimate, paleodrainage, and paleoaltimetry: Geosphere, v. 8, n. 6, p. 1177–1206, https://doi.org/10.1130/GES00801.1
Chapin, C. E., 2012, Origin of the Colorado Mineral Belt: Geosphere, v. 8, n. 1, p. 28–43, https://doi.org/10.1130/GES00694.1
Chew, D. M., and Donelick, R. A., 2012, Combined apatite fission-track and U-Pb dating by LA-ICP-MS and its application in apatite provenance analysis, *in* Sylvester, P., editor, Quantitative Mineralogy and Microanalysis of Sediments and Sedimentary Rocks: Mineralogical Association of Canada, Short Course 42, p. 219–247.
Condie, K. C., and Selverstone, J., 1999, The Crust of the Colorado Plateau: New Views of an Old Arc: The Journal of Geology, v. 107, n. 4, p. 387–397, https://doi.org/10.1086/314363
Condie, K. C., Latysh, N., Van Schmus, W. R., Kozuch, M., and Selverstone, J., 1999, Geochemistry, Nd and Sr isotopes, and U/Pb zircon ages of granitoid and metasedimentary xenoliths from the Navajo volcanic field, Four Corners area, Southwestern United States: Chemical Geology, v. 156, n. 1–4, p. 95–133, https://doi.org/10.1016/S0009-2541(98)00176-4
Coney, P. J., and Reynolds, S. J., 1977, Cordilleran Benioff zones: Nature, v. 270, p. 403–406, https://doi.org/10.1038/270403a0
Cook, K. L., Whipple, K. X., Heimsath, A. M., and Hanks, T. C., 2009, Rapid incision of the Colorado River in Glen Canyon - insights from channel profiles, local incision rates, and modeling of lithologic controls: Earth Surface Processes and Landforms, v. 34, n. 7, https://doi.org/10.1002/esp.1790
Copeland, P., Currie, C. A., Lawton, T. F., and Murphy, M. A., 2017, Location, location, location: The variable lifespan of the Laramide orogeny: Geology, v. 45, n. 3, p. 223–226, https://doi.org/10.1130/G38810.1
Crow, R., Karlstrom, K., Asmerom, Y., Schmandt, B., Polyak, V., and Dufrane, S. A., 2011, Shrinking of the Colorado Plateau via lithospheric mantle erosion: Evidence from Nd and Sr isotopes and geochronology of Neogene basalts: Geology, v. 39, n. 1, p. 27–30, https://doi.org/10.1130/G31611.1
Crowley, J. L., Schmitz, M. D., Bowring, S. A., Williams, M. L., and Karlstrom, K. E., 2006, U–Pb and Hf isotopic analysis of zircon in lower crustal xenoliths from the Navajo volcanic field: 1.4 Ga mafic magmatism and metamorphism beneath the Colorado Plateau: Contributions to Mineralogy and Petrology, v. 151, n. 3, p. 313–330, https://doi.org/10.1007/s00410-006-0061-z
Darling, A. L., Karlstrom, K. E., Granger, D. E., Aslan, A., Kirby, E., Ouimet, W. B., Lazear, G. D., Coblentz, D. D., and Cole, R. D., 2012, New incision rates along the Colorado River system based on cosmogenic burial dating of terraces: Implications for regional controls on Quaternary incision: Geosphere, v. 8, n. 5, p. 1020–1041, https://doi.org/10.1130/GES00724.1
Davis, J. M., Elston, W. E., and Hawkesworth, C. J., 1993, Basic and intermediate volcanism of the Mogollon-Datil volcanic field: Implications for mid-Tertiary tectonic transitions in southwestern New Mexico, USA, *in* Prichard, H. M., Alabaster, T., Harris, N. B. W., and Neary, C. R., editors, Magmatic Processes and Plate Tectonics: Geological Society, London, Special Publications, v. 76, p. 469–488, https://doi.org/10.1144/GSL.SP.1993.076.01.25
Davis, S. J., Mix, H. T., Wiegand, B. A., Carroll, A. R., and Chamberlain, C. P., 2009, Synorogenic evolution of large-scale drainage patterns: Isotope paleohydrology of sequential Laramide basins: American Journal of Science, v. 309, n. 7, p. 549–602, https://doi.org/10.2475/07.2009.02
DeCelles, P. G., 2004, Late Jurassic to Eocene evolution of the Cordilleran thrust belt and foreland basin system, western USA: American Journal of Science, v. 304, n. 2, p. 105–168, https://doi.org/10.2475/ajs.304.2.105
Dickinson, W. R., 2013, Rejection of the lake spillover model for initial incision of the Grand Canyon, and discussion of alternatives: Geosphere, v. 9, n. 1, p. 1–20, https://doi.org/10.1130/GES00839.1
Dickinson, W. R., and Snyder, W. S., 1978, Plate tectonics of the Laramide orogeny, *in* Matthews III, V., editor, Laramide folding associated with basement block faulting in the western United States: Geological Society of America Memoir 151, p. 355–366, https://doi.org/10.1130/MEM151-p355
Dickinson, W. R., Klute, M. A., Hayes, M. J., Janecke, S. U., Lundin, E. R., McKittrick, M. A., and Olivares, M. D., 1988, Paleogeographic and paleotectonic setting of Laramide sedimentary basins in the central Rocky Mountain region: GSA Bulletin, v. 100, n. 7, p. 1023–1039, https://doi.org/10.1130/0016-7606(1988)100<1023:PAPSOL>2.3.CO;2
Dorsey, R. J., and Lazear, G., 2013, A post–6 Ma sediment budget for the Colorado River: Geosphere, v. 9, n. 4, p. 781–791, https://doi.org/10.1130/GES00784.1
Dorsey, R. J., Fluette, A., McDougall, K., Housen, B. A., Janecke, S. U., Axen, G. J., and Shirvell, C. R., 2007, Chronology of Miocene–Pliocene deposits at Split Mountain Gorge, Southern California: A record of regional tectonics and Colorado River evolution: Geology, v. 35, n. 1, p. 57, https://doi.org/10.1130/G23139A.1
Dumitru, T. A., Gans, P. B., Foster, D. A., and Miller, E. L., 1991, Refrigeration of the western Cordilleran lithosphere during Laramide shallow-angle subduction: Geology, v. 19, n. 11, p. 1145, https://doi.org/10.1130/0091-7613(1991)019<1145:ROTWCL>2.3.CO;2
Dumitru, T. A., Duddy, I. R., and Green, P. F., 1994, Mesozoic-Cenozoic burial, uplift, and erosion history of the west-central Colorado Plateau: Geology, v. 22, n. 6, p. 499–502, https://doi.org/10.1130/0091-7613(1994)022<0499:MCBUAE>2.3.CO;2
Dutton, C. E., 1882, Tertiary history of the Grand Cañon district: United States Geological Survey Monograph 2, 315 p.
Elston, D. P., and Young, R. A., 1991, Cretaceous-Eocene (Laramide) landscape development and Oligocene-Pliocene drainage reorganization of transition zone and Colorado Plateau, Arizona: Journal of Geophysical Research-Solid Earth, v. 96, n. B7, p. 12,389–12,406, https://doi.org/10.1029/90JB01978
Emmons, S. F., 1897, The origin of Green River: Science, v. 6, n. 131, p. 20–21, C https://doi.org/10.1126/science.6.131.19

English, J. M., Johnston, S. T., and Wang, K., 2003, Thermal modelling of the Laramide orogeny: Testing the flat-slab subduction hypothesis: Earth and Planetary Science Letters, v. 214, n. 3–4, p. 619–632, https://doi.org/10.1016/S0012-821X(03)00399-6

Erdman, M. E., Lee, C.-T.A., Levander, A., and Jiang, H., 2016, Role of arc magmatism and lower crustal foundering in controlling elevation history of the Nevadaplano and Colorado Plateau: A case study of pyroxenitic lower crust from central Arizona, USA: Earth and Planetary Science Letters, v. 439, n. C, p. 48–57, https://doi.org/10.1016/j.epsl.2016.01.032

Farley, K. A., 2000, Helium diffusion from apatite: General behavior as illustrated by Durango fluorapatite: Journal of Geophysical Research-Solid Earth, v. 105, n. B2, p. 2903–2914, https://doi.org/10.1029/1999JB900348

Farley, K. A., Shuster, D. L., and Ketcham, R. A., 2011, U and Th zonation in apatite observed by laser ablation ICPMS, and implications for the (U–Th)/He system: Geochimica et Cosmochimica Acta, n. 75, n. 16, p. 4515–4530, https://doi.org/10.1016/j.gca.2011.05.020

Farmer, G. L., Bailley, T., and Elkins-Tanton, L. T., 2008, Mantle source volumes and the origin of the mid-Tertiary ignimbrite flare-up in the southern Rocky Mountains, western U.S.: Lithos, v. 102, n. 1–2, p. 279–294, https://doi.org/10.1016/j.lithos.2007.08.014

Flowers, R. M., and Farley, K. A., 2012, Apatite $^{4}He/^{3}He$ and (U-Th)/He Evidence for an Ancient Grand Canyon: Science, v. 338, n. 6114, p. 1616–1619, https://doi.org/10.1126/science.1229390

Flowers, R. M., and Kelley, S. A., 2011, Interpreting data dispersion and "inverted" dates in apatite (U–Th)/He and fission-track datasets: An example from the US midcontinent: Geochimica et Cosmochimica Acta, v. 75, n. 18, p. 5169–5186, https://doi.org/10.1016/j.gca.2011.06.016

Flowers, R. M., Shuster, D. L., Wernicke, B. P., and Farley, K. A., 2007, Radiation damage control on apatite (U-Th)/He dates from the Grand Canyon region, Colorado Plateau: Geology, v. 35, n. 5, p. 447–450, https://doi.org/10.1130/G23471A.1

Flowers, R. M., Wernicke, B. P., and Farley, K. A., 2008, Unroofing, incision, and uplift history of the southwestern Colorado Plateau from apatite (U-Th)/He thermochronometry: GSA Bulletin, v. 120, n. 5–6, p. 571–587, https://doi.org/10.1130/B26231.1

Flowers, R. M., Ketcham, R. A., Shuster, D. L., and Farley, K. A., 2009, Apatite (U–Th)/He thermochronometry using a radiation damage accumulation and annealing model: Geochimica et Cosmochimica Acta, v. 73, n. 8, p. 2347–2365, https://doi.org/10.1016/j.gca.2009.01.015

Flowers, R. M., Farley, K. A., and Ketcham, R. A., 2015, A reporting protocol for thermochronologic modeling illustrated with data from the Grand Canyon: Earth and Planetary Science Letters, v. 432, n. C, p. 425–435, https://doi.org/10.1016/j.epsl.2015.09.053

Fox, M., and Shuster, D. L., 2014, The influence of burial heating on the (U–Th)/He system in apatite: Grand Canyon case study: Earth and Planetary Science Letters, v. 397, p. 174–183, https://doi.org/10.1016/j.epsl.2014.04.041

Fox, M., Tripathy-Lang, A., Shuster, D. L., Winn, C., Karlstrom, K., and Kelley, S., 2017, Westernmost Grand Canyon incision: Testing thermochronometric resolution: Earth and Planetary Science Letters, v. 474, p. 248–256, https://doi.org/10.1016/j.epsl.2017.06.049

Galbraith, R. F., 1981, On statistical models for fission track counts: Mathematical Geology, v. 13, n. 6, p. 471–478, https://doi.org/10.1007/BF01034498

——— 2005, Statistics for Fission Track Analysis: Boca Raton, Florida, Chapman & Hall/CRC, 240 p., https://doi.org/10.1201/9781420034929

Galloway, W. E., Whiteaker, T. L., and Ganey-Curry, P., 2011, History of Cenozoic North American drainage basin evolution, sediment yield, and accumulation in the Gulf of Mexico basin: Geosphere, v. 7, n. 4, p. 938–973, https://doi.org/10.1130/GES00647.1

Gautheron, C., Tassan-Got, L., Barbarand, J., and Pagel, M., 2009, Effect of alpha-damage annealing on apatite (U–Th)/He thermochronology: Chemical Geology, v. 266, n. 3–4, p. 157–170, https://doi.org/10.1016/j.chemgeo.2009.06.001

Gautheron, C., Tassan-Got, L., Ketcham, R. A., and Dobson, K. J., 2012, Accounting for long alpha-particle stopping distances in (U–Th–Sm)/He geochronology: 3D modeling of diffusion, zoning, implantation, and abrasion: Geochimica et Cosmochimica Acta, v. 96, n. 96, p. 44–56, https://doi.org/10.1016/j.gca.2012.08.016

Gautheron, C., Barbarand, J., Ketcham, R. A., Tassan-Got, L., van der Beek, P., Pagel, M., Pinna-Jamme, R., Couffignal, F., and Fialin, M., 2013, Chemical influence on α-recoil damage annealing in apatite: Implications for (U–Th)/He dating: Chemical Geology, v. 351, n. C, p. 257–267, https://doi.org/10.1016/j.chemgeo.2013.05.027

Gehrels, G. E., Valencia, V. A., and Ruiz, J., 2008, Enhanced precision, accuracy, efficiency, and spatial resolution of U-Pb ages by laser ablation-multicollector-inductively coupled plasma-mass spectrometry: Geochemistry, Geophysics, Geosystems, v. 9, n. 3, p. 1–13, https://doi.org/10.1029/2007GC001805

Gilbert, G. K., 1877, Report on the Geology of the Henry Mountains: Washington, D. C., Government Printing Office, 169 p., https://doi.org/10.3133/70039916

Gleadow, A J. W., 1981, Fission-Track Dating Methods: What Are the Real Alternatives: Nuclear Tracks and Radiation Measurements, v. 5, n. 1–2, p. 3–14, https://doi.org/10.1016/0191-278X(81)90021-4

Goldstrand, P., 1994, Tectonic development of Upper Cretaceous to Eocene strata of southwestern Utah: GSA Bulletin, v. 106, n. 1, p. 145, https://doi.org/10.1130/0016-7606(1994)106<0145:TDOUCT>2.3.CO;2

Gonzales, D. A., and Lake, E. T., 2017, Geochemical constraints on mantle-melt sources for Oligocene to Pleistocene mafic rocks in the Four Corners region, USA: Geosphere, v. 13, n. 1, p. 201–226, https://doi.org/10.1130/GES01314.1

Green, P. F., Duddy, I. R., Laslett, G. M., Hegarty, K. A., Gleadow, A. J. W., and Lovering, J. F., 1989, Thermal

annealing of fission tracks in apatite 4. Quantitative modelling techniques and extension to geological timescales: Chemical Geology, v. 79, n. 2, p. 155–182, https://doi.org/10.1016/0168-9622(89)90018-3
Hansen, W. R., 1986, Neogene Tectonic and Geomorphology of the Eastern Uinta Mountains in Utah, Colorado, and Wyoming: USGS Professional Paper, v. 1356, p. 78, https://doi.org/10.3133/pp1356
Hintze, L. F., and Kowallis, B. J., 2009, Geologic History of Utah: A Fieldguide to Utah's Rocks: Provo, Utah, Brigham Young University Department of Geology, 181 p.
Hintze, L. F., Willis, G. C., Laes, D. Y. M., Sprinkel, D. A., and Brown, K. D., 2000, Digital Geologic Map of Utah: Utah Geological Survey, scale 1:500,000.
Hoffman, M. D., ms, 2009, Mio-Pliocene erosional exhumation of the central Colorado Plateau, eastern Utah: New insights from apatite (U-Th)/He thermochronometry: Lawrence, Kansas, University of Kansas, M. S. thesis, 185 p.
Hoffman, M. D., Stockli, D. F., Kelley, S. A., Pederson, J. L., and Lee, J., 2011, Mio-Pliocene Erosional Exhumation of the Central Colorado Plateau, Eastern Utah—New Insights from Apatite (U-Th)/He Thermochronometry, *in* Beard, L. S., Karlstrom, K. E., Young, R. A., and Billingsley, G. H., editors, CRevolution 2—Origin and Evolution of the Colorado River System, Workshop Abstracts: US. Geological Survey Open File Report 2011-1210, p. 132–136.
Holm, R. F., 2001, Cenozoic paleogeography of the central Mogollon Rim-southern Colorado Plateau region, Arizona, revealed by Tertiary gravel deposits, Oligocene to Pleistocene lava flows, and incised streams: GSA Bulletin, v. 113, n. 11, p. 1467–1485, https://doi.org/10.1130/0016-7606(2001)113<1467:CPOTCM>2.0.CO;2
House, M. A., Kelley, S. A., and Roy, M., 2003, Refining the footwall cooling history of a rift flank uplift, Rio Grande rift, New Mexico: Tectonics, v. 22, n. 5, p. 1–14, https://doi.org/10.1029/2002TC001418
Humphreys, E., 2009, Relation of flat subduction to magmatism and deformation in the western United States, *in* Kay, S. M., Ramos, V. A, and Dickinson, W. R., editors, Backbone of the Americas: Shallow Subduction, Plateau Uplift, and Ridge and Terrane Collision: Geological Society of America Memoir 204, p. 85–98, https://doi.org/10.1130/2009.1204(04)
Humphreys, E., Hessler, E., Dueker, K., Farmer, C. L., Erslev, E., and Atwater, T., 2003, How Laramide-age hydration of North American lithosphere by the Farallon slab controlled subsequent activity in the western United States: International Geology Review, v. 45, n. 7, p. 575–595, https://doi.org/10.2747/0020-6814.45.7.575
Humphreys, E. D., 1995, Post-Laramide removal of the Farallon slab, western United States: Geology, v. 23, n. 11, p. 987–990, https://doi.org/10.1130/0091-7613(1995)023<0987:PLROTF>2.3.CO;2
Hunt, C. B., 1956, Cenozoic Geology of the Colorado Plateau: Geological Survey Professional Paper 279, 97 p., https://doi.org/10.3133/pp279
——— 1958, Structural and Igneous Geology of theLa Sal Mountains, Utah: Geological Survey Professional Paper 294-I, 68 p., https://doi.org/10.3133/pp294I
——— 1969, Geologic History of the Colorado River, *in* The Colorado River Region and John Wesley Powell: United States Geological Survey Professional Paper 669-C, p. 59–130, https://doi.org/10.3133/pp669C
Hunt, C. B., Averitt, P., and Miller, R. L., 1953, Geology and geography of the Henry Mountains region, Utah: A survey and restudy of one of the classic areas in geology: United States Geologic Survey Professional Paper 228, 234 p., https://doi.org/10.3133/pp228
Huntington, K. W., Wernicke, B. P., and Eiler, J. M., 2010, Influence of climate change and uplift on Colorado Plateau paleotemperatures from carbonate clumped isotope thermometry: Tectonics v. 29, n. 3, https://doi.org/10.1029/2009TC002449
Huntoon, J. E., Hansley, P. L., and Naeser, N. D., 1999, The search for a source rock for the giant Tar Sand Triangle accumulation, southeastern Utah: AAPG Bulletin, v. 83, n. 3, p. 467–495.
Hurford, A. J., 1990, Standardization of fission track dating calibration: Recommendation by the Fission Track Working Group of the IUGS Subcommission on Geochronology: Chemical Geology; Isotope Geoscience Section, v. 80, n. 2, p. 171–178, https://doi.org/10.1016/0168-9622(90)90025-8
Hurford, A. J., and Green, P. F., 1983, The zeta age calibration of fission-track dating: Isotope Geoscience, v. 1, p. 285–317, https://doi.org/10.1016/S0009-2541(83)80026-6
Jackson, M. D., and Pollard, D. D., 1988, The laccolith-stock controversy: New results from the southern Henry Mountains, Utah: GSA Bulletin, v. 100, n. 1, p. 117–139, https://doi.org/10.1130/0016-7606(1988)100<0117:TLSCNR>2.3.CO;2
Johnson, A. M., and Pollard, D. D., 1973, Mechanics of growth of some laccolithic intrusions in the Henry mountains, Utah, I: Field observations, Gilbert's model, physical properties and flow of the magma: Tectonophysics, v. 18, n. 3–4, p. 261–309, https://doi.org/10.1016/0040-1951(73)90050-4
Johnson, C. M., 1991, Large-scale crust formation and lithosphere modification beneath Middle to Late Cenozoic calderas and volcanic fields, western North America: Journal of Geophysical Research-Solid Earth, v. 96, n. B8, p. 13,485–13,507, https://doi.org/10.1029/91JB00304
Johnson, J. P. L., Whipple, K. X., and Sklar, L. S., 2010, Contrasting bedrock incision rates from snowmelt and flash floods in the Henry Mountains, Utah: Geological Society of America Bulletin, v. 122, n. 9–10, p. 1600–1615, https://doi.org/10.1130/B30126.1
Johnstone, S., Hourigan, J., and Gallagher, C., 2013, LA-ICP-MS depth profile analysis of apatite: Protocol and implications for (U–Th)/He thermochronometry: Geochimica et Cosmochimica Acta, n. 109, p. 143–161, https://doi.org/10.1016/j.gca.2013.01.004
Jones, C. H., Farmer, G. L., Sageman, B., and Zhong, S., 2011, Hydrodynamic mechanism for the Laramide orogeny: Geosphere, v. 7, n. 1, p. 183–201, https://doi.org/10.1130/GES00575.1
Jones, C. H., Mahan, K. H., Butcher, L. A., Levandowski, W. B., and Farmer, G. L., 2015, Continental uplift through crustal hydration: Geology, v. 43, n. 4, p. 355–358, https://doi.org/10.1130/G36509.1
Karlstrom, K. E., Coblentz, D., Dueker, K., Ouimet, W., Kirby, E., Van Wijk, J., Schmandt, B., Kelley, S., Lazear, G., Crossey, L. J., Crow, R., Aslan, A., Darling, A., Aster, R., MacCarthy, J., Hansen, S. M.,

Stachnik, J., Stockli, D. F., Garcia, R. V., Hoffman, M., McKeon, R., Feldman, J., Heizler, M., Donahue, M. S., and the CREST Working Group, 2012, Mantle-driven dynamic uplift of the Rocky Mountains and Colorado Plateau and its surface response: Toward a unified hypothesis: Lithosphere, v. 4, n. 1, p. 3–22, https://doi.org/10.1130/L150.1

Karlstrom, K. E., Lee, J. P., Kelley, S. A., Crow, R. S., Crossey, L. J., Young, R. A., Lazear, G., Beard, L. S., Ricketts, J. W., Fox, M., and Shuster, D. L., 2014, Formation of the Grand Canyon 5 to 6 million years ago through integration of older palaeocanyons: Nature Geoscience, v. 7, p. 239–244, https://doi.org/10.1038/ngeo2065

Karlstrom, K. E., Crossey, L. J., Embid, E., Crow, R., Heizler, M., Hereford, R., Beard, L. S., Ricketts, J. W., Cather, S., and Kelley, S., 2017, Cenozoic incision history of the Little Colorado River: Its role in carving Grand Canyon and onset of rapid incision in the past *ca.* 2 Ma in the Colorado River System: Geosphere, v. 13, n. 1, p. 49–81, https://doi.org/10.1130/GES01304.1

Kelley, S. A., and Karlstrom, K. E., 2012, The Laramide and post-Laramide uplift and erosional history of the eastern Grand Canyon: Evidence from apatite fission-track thermochronology, *in* Timmons, J. M., and Karlstrom, K. E. editors., Grand Canyon Geology: Two Billion Years of Earth's History: Geological Society of America Special Paper 489, p. 109–117, https://doi.org/10.1130/2012.2489(07)

Ketcham, R. A., 2005, Forward and inverse modeling of low-temperature thermochronometry data: Reviews in Mineralogy and Geochemistry, v. 58, n. 1, p. 275–314, https://doi.org/10.2138/rmg.2005.58.11

Ketcham, R. A., Carter, A., Donelick, R. A., Barbarand, J., and Hurford, A. J., 2007, Improved modeling of fission-track annealing in apatite: American Mineralogist, v. 92, n. 5–6, p. 799–810, https://doi.org/10.2138/am.2007.2281

Ketcham, R. A., Gautheron, C., and Tassan-Got, L., 2011, Accounting for long alpha-particle stopping distances in (U-Th-Sm)/He geochronology: Refinement of the baseline case: Geochimica et Cosmochimica Acta, v. 75, n. 24, p. 7779–7791, https://doi.org/10.1016/j.gca.2011.10.011

Kimbrough, D. L., Grove, M., Gehrels, G. E., Dorsey, R. J., Howard, K. A., Lovera, O., Aslan, A., House, P. K., and Pearthree, P. A., 2015, Detrital zircon U-Pb provenance of the Colorado River: A 5 m.y. record of incision into cover strata overlying the Colorado Plateau and adjacent regions: Geosphere, v. 11, n. 6, p. 1719–1748, https://doi.org/10.1130/GES00982.1

Lake, E. T., and Farmer, G. L., 2015, Oligo-Miocene mafic intrusions of the San Juan Volcanic Field, southwestern Colorado, and their relationship to voluminous, caldera-forming magmas: Geochimica et Cosmochimica Acta, v. 157, p. 86–108, https://doi.org/10.1016/j.gca.2015.02.020

Landman, R. L., Flowers, R. M., and Kelley, S. A., 2016, Lithospheric hydration gradient and elevated Oligocene heat flow across the transition between the North American cordillera and cratonic interior: Geological Society of America Abstracts with Programs, v. 48, n. 7, https://doi.org/10.1130/abs/2016AM-283290

Laughlin, A. W., Aldrich Jr., M. J., Shafiquallah, M., and Husler, J., 1986, Tectonic implications of the age, composition, and orientation of lamprophyre dikes, Navajo volcanic field, Arizona: Earth and Planetary Science Letters, v. 76, n. 3–4, p. 361–374, https://doi.org/10.1016/0012-821X(86)90087-7

Lazear, G., Karlstrom, K., Aslan, A., and Kelley, S., 2013, Denudation and flexural isostatic response of the Colorado Plateau and southern Rocky Mountains region since 10 Ma: Geosphere, v. 9, n. 4, p. 792–814, https://doi.org/10.1130/GES00836.1

Lee, C. T., Yin, Q. Z., Rudnick, R. L., and Jacobsen, S. B., 2001, Preservation of ancient and fertile lithospheric mantle beneath the southwestern United States: Nature, v. 411, n. 6833, p. 69–73, https://doi.org/10.1038/35075048

Lee, J. P., Stockli, D. F., Kelley, S. A., Pederson, J. L., Karlstrom, K. E., and Ehlers, T. A., 2013, New thermochronometric constraints on the Tertiary landscape evolution of the central and eastern Grand Canyon, Arizona: Geosphere, v. 9, n. 2, p. 216–228, https://doi.org/10.1130/GES00842.1

Leonard, E. M., Hubbard, M. S., Kelley, S. A., Evanoff, E., Siddoway, C. S., Oviatt, C. G., Heizler, M., and Timmons, M., 2002, High Plains to Rio Grande rift: Late Cenozoic evolution of central Colorado: GSA Field Guides, v. 3, p. 59–93, https://doi.org/10.1130/0-8137-0003-5.59

Levander, A., Schmandt, B., Miller, M. S., Liu, K., Karlstrom, K. E., Crow, R. S., Lee, C.-T.A., and Humphreys, E. D., 2011, Continuing Colorado plateau uplift by delamination-style convective lithospheric downwelling: Nature, v. 472, p. 461–465, https://doi.org/10.1038/nature10001

Lipman, P. W., 2007, Incremental assembly and prolonged consolidation of Cordilleran magma chambers: Evidence from the Southern Rocky Mountain volcanic field: Geosphere, v. 3, n. 1, p. 42–70, https://doi.org/10.1130/GES00061.1

Lipman, P. W., and Glazner, A. F., 1991, Introduction to middle Tertiary cordilleran volcanism: Magma sources and relations to regional tectonics: Journal of Geophysical Research-Solid Earth, v. 96, n. B8, p. 13193–13199, https://doi.org/10.1029/91JB01397

Liu, L., and Gurnis, M., 2010, Dynamic subsidence and uplift of the Colorado Plateau: Geology, v. 38, n. 7, p. 663–666, https://doi.org/10.1130/G30624.1

Liu, L., Gurnis, M., Seton, M., Saleeby, J., Müller, R. D., and Jackson, J. M., 2010, The role of oceanic plateau subduction in the Laramide orogeny: Nature Geoscience, v. 3, n. 4, p. 353–357, https://doi.org/10.1038/ngeo829

Ludwig, K. R., 2008, Isoplot 3.60: Berkeley, California, Berkeley Geochronology Center, Special Publication, 77 p.

McIntosh, W. C., Chapin, C. E., Ratté, J. C., and Sutter, J. F., 1992, Time-stratigraphic framework for the Eocene-Oligocene Mogollon-Datil volcanic field, southwest New Mexico: GSA Bulletin, v. 104, n. 7, p. 851–871, https://doi.org/10.1130/0016-7606(1992)104<0851:TSFFTE>2.3.CO;2

McKeon, R. E., Zeitler, P. K., Pazzaglia, F. J., Idleman, B. D., and Enkelmann, E., 2013, Decay of an old orogen: Inferences about Appalachian landscape evolution from low-temperature thermochronology: GSA Bulletin, v. 126, n. 1–2, p. 31–46, https://doi.org/10.1130/B30808.1

McQuarrie, N., and Chase, C., 2000, Raising the Colorado plateau: Geology, v. 28, n. 1, p. 91–94, https://doi.org/10.1130/0091-7613(2000)028<0091:RTCP>2.3.CO;2
Minder, J. R., Mote, P. W., and Lundquist, J. D., 2010, Surface temperature lapse rates over complex terrain: Lessons from the Cascade Mountains: Journal of Geophysical Research-Atmospheres, v. 115, n. D14, https://doi.org/10.1029/2009JD013493
Morgan, P., and Swanberg, C. A., 1985, On the Cenozoic uplift and tectonic stability of the Colorado Plateau: Journal of Geodynamics, v. 3, n. 1–2, p. 39–63, https://doi.org/10.1016/0264-3707(85)90021-3
Moucha, R., Forte, A. M., Rowley, D. B., Mitrovica, J. X., Simmons, N. A., and Grand, S. P., 2009, Deep mantle forces and the uplift of the Colorado Plateau: Geophysical Research Letters, v. 36, n. 19, p. L19310, https://doi.org/10.1029/2009GL039778
Murray, K. E., Orme, D. A., and Reiners, P. W., 2014, Effects of U–Th-rich grain boundary phases on apatite helium ages: Chemical Geology, v. 390, p. 135–151, https://doi.org/10.1016/j.chemgeo.2014.09.023
Murray, K. E., Reiners, P. W., and Thomson, S. N., 2016, Rapid Pliocene–Pleistocene erosion of the central Colorado Plateau documented by apatite thermochronology from the Henry Mountains: Geology, v. 44, n. 6, p. 483–486, https://doi.org/10.1130/G37733.1
Murray, K. E., Braun, J., and Reiners, P. W., 2018, Toward Robust Interpretation of Low-Temperature Thermochronometers in Magmatic Terranes: Geochemistry, Geophysics, Geosystems, v. 19, n. 10, p. 3739–3763, https://doi.org/10.1029/2018GC007595
Naeser, C. W., Duddy, I. R., Elston, D. P., Dumitru, T. A., and Green, P. F., 1989, Fission-track dating: Ages for Cambrian strata and Laramide and post-Middle Eocene cooling events from the Grand Canyon, Arizona, *in* Elston, D. P., Billingsley, G. H., and Young, R. A. editors, Geology of Grand Canyon, Northern Arizona (with Colorado River Guides): Lee Ferry to Pierce Ferry, Arizona: Washington, D. C., American Geophysical Union, Field Trip Guidebooks, v. 115, p. 139–144, https://doi.org/10.1029/FT115p0139
Nelson, S. T., and Davidson, J. P., 1993, Interactions Between Mantle-Derived Magmas and Mafic Crust, Henry Mountains, Utah: Journal of Geophysical Research-Solid Earth, v. 98, n. B2, p. 1837–1852, https://doi.org/10.1029/92JB02689
Nelson, S. T., Davidson, J. P., and Sullivan, K. R., 1992, New age determinations of central Colorado Plateau laccoliths, Utah: Recognizing disturbed K-Ar systematics and re-evaluating tectonomagmatic relationships: Geological Society of America Bulletin, v. 104, n. 12, p. 1547–1560, https://doi.org/10.1130/0016-7606(1992)104<1547:NADOCC>2.3.CO;2
Pederson, J. L., and Tressler, C., 2012, Colorado River long-profile metrics, knickzones and their meaning: Earth and Planetary Science Letters, v. 345–348, n. C, p. 171–179, https://doi.org/10.1016/j.epsl.2012.06.047
Pederson, J. L., Mackley, R. D., and Eddleman, J. L., 2002, Colorado Plateau uplift and erosion evaluated using GIS: GSA Today, v. 12, n. 8, https://doi.org/10.1130/1052-5173(2002)012<0004:CPUAEE>2.0.CO;2
Pederson, J. L., Cragun, W. S., Hidy, A. J., Rittenour, T. M., and Gosse, J. C., 2013, Colorado River chronostratigraphy at Lee"s Ferry, Arizona, and the Colorado Plateau bull's-eye of incision: Geology, v. 41, n. 4, p. 427–430, https://doi.org/10.1130/G34051.1
Peirce, H. W., Damon, P. E., and Shafiquallah, M., 1979, An Oligocene (?) Colorado Plateau edge in Arizona: Tectonophysics, v. 61, n. 1–3, p. 1–24, https://doi.org/10.1016/0040-1951(79)90289-0
Pelletier, J. D., 2009, The impact of snowmelt on the late Cenozoic landscape of the southern Rocky Mountains, USA: GSA Today, v. 19, n. 7, p. 4–11, https://doi.org/10.1130/GSATG44A.1
Perry, F. V., DePaolo, D. J., and Baldridge, W. S., 1993, Neodymium isotopic evidence for decreasing crustal contributions to Cenozoic ignimbrites of the western United States: Implications for the thermal evolution of the Cordilleran crust: GSA Bulletin, v. 105, n. 7, p. 872–882, https://doi.org/10.1130/0016-7606(1993)105<0872:NIEFDC>2.3.CO;2
Pollard, D., and Johnson, A. M., 1973, Mechanics of growth of some laccolithic intrusions in the Henry mountains, Utah, II: Bending and failure of overburden layers and sill formation: Tectonophysics, v. 18, n. 3–4, p. 311–354, https://doi.org/10.1016/0040-1951(73)90051-6
Porter, R., Hoisch, T., and Holt, W. E., 2017, The role of lower-crustal hydration in the tectonic evolution of the Colorado Plateau: Tectonophysics, v. 712–713, p. 221–231, https://doi.org/10.1016/j.tecto.2017.05.025
Powell, J. W., 1875, The Exploration of the Colorado River of the West and Its Tributaries: Washington, D. C., U.S. Government Printing Office, Monograph, 291 p., https://doi.org/10.3133/70039238
Reiners, P. W., 2005, Zircon (U-Th)/He thermochronometry: Reviews in Mineralogy and Geochemistry, v. 58, p. 151–179, https://doi.org/10.2138/rmg.2005.58.6
Reiners, P. W., and Farley, K. A., 2001, Influence of crystal size on apatite (U-Th)/He thermochronology: An example from the Bighorn Mountains, Wyoming: Earth and Planetary Science Letters, v. 188, n. 3–4, p. 413–420, https://doi.org/10.1016/S0012-821X(01)00341-7
Reiners, P. W., Spell, T. L., Nicolescu, S., and Zanetti, K. A., 2004, Zircon (U-Th)/He thermochronometry: He diffusion and comparisons with $^{40}Ar/^{39}Ar$ dating: Geochimica et Cosmochimica Acta, v. 68, n. 8, p. 1857–1887, https://doi.org/10.1016/j.gca.2003.10.021
Reiners, P. W., Chan, M. A., and Evenson, N. S., 2014, (U-Th)/He geochronology and chemical compositions of diagenetic cement, concretions, and fracture-filling oxide minerals in Mesozoic sandstones of the Colorado Plateau: GSA Bulletin, v. 126, n. 9–10, p. 1363–1383, https://doi.org/10.1130/B30983.1
Ricketts, J. W., Kelley, S. A., Karlstrom, K. E., Schmandt, B., Donahue, M. S., and van Wijk, J., 2016, Synchronous opening of the Rio Grande rift along its entire length at 25–10 Ma supported by apatite (U-Th)/He and fission-track thermochronology, and evaluation of possible driving mechanisms: Geological Soceity of America Bulletin, v. 128, n. 3–4, p. 397–424, https://doi.org/10.1130/B31223.1
Roberts, G. G., White, N. J., Martin-Brandis, G. L., and Crosby, A. G., 2012, An uplift history of the Colorado

Plateau and its surroundings from inverse modeling of longitudinal river profiles: Tectonics, v. 31, n. 4, p. n/a–n/a, https://doi.org/10.1029/2012TC003107
Roden, M. F., Smith, D., and McDowell, F. W., 1979, Age and extent of potassic volcanism on the Colorado Plateau: Earth and Planetary Science Letters, v. 43, n. 2, p. 279–284, https://doi.org/10.1016/0012-821X(79)90212-7
Rowley, P., Cunningham, C., Steven, T., Mehnert, H., and Naeser, C., 1998, Cenozoic igneous and tectonic setting of the Marysvale volcanic field and its relation to other igneous centers in Utah and Nevada, *in* Friedman, J. D., and Huffman, A. C., Jr., coordinators, Laccolith complexes of southeastern Utah—Time of emplacement and tectonic setting—Workshop proceedings: US Geological Survey Bulletin, v. 2158, p. 167–202.
Roy, M., Kelley, S., Pazzaglia, F., Cather, S., and House, M., 2004, Middle Tertiary buoyancy modification and its relationship to rock exhumation, cooling, and subsequent extension at the eastern margin of the Colorado Plateau: Geology, v. 32, n. 10, p. 925–928, https://doi.org/10.1130/G20561.1
Roy, M., Jordan, T. H., and Pederson, J., 2009, Colorado Plateau magmatism and uplift by warming of heterogeneous lithosphere: Nature, v. 459, n. 7249, p. 978–982, https://doi.org/10.1038/nature08052
Rønnevik, C., Ksienzyk, A. K., Fossen, H., and Jacobs, J., 2017, Thermal evolution and exhumation history of the Uncompahgre Plateau (northeastern Colorado Plateau), based on apatite fission track and (U-Th)-He thermochronology and zircon U-Pb dating: Geosphere, v. 13, n. 2, p. 518–537, https://doi.org/10.1130/GES01415.1
Schulze, D. J., Davis, D. W., Helmstaedt, H., and Joy, B., 2015, Timing of the Cenozoic "Great Hydration" event beneath the Colorado Plateau: Th-Pb dating of monazite in Navajo volcanic field metamorphic eclogite xenoliths: Geology, v. 43, n. 8, p. 727–730, https://doi.org/10.1130/G36932.1
Sears, J. W., 2013, Late Oligocene–early Miocene Grand Canyon: A Canadian connection?: GSA Today, v. 23, n. 11, p. 4–10, https://doi.org/10.1130/GSATG178A.1
Semken, S., 2003, Black rocks protruding up: the Navajo Volcanic Field, *in* Geology of the Zuni Plateau: New Mexico Geological Society Guidebook, 54th Field Conference, p. 133–138.
Shuster, D. L., Flowers, R. M., and Farley, K. A., 2006, The influence of natural radiation damage on helium diffusion kinetics in apatite: Earth and Planetary Science Letters, n. 249, n. 3–4, p. 148–161, https://doi.org/10.1016/j.epsl.2006.07.028
Snyder, W. S., Dickinson, W. R., and Silberman, M. L., 1976, Tectonic implications of space-time patterns of Cenozoic magmatism in the western United States: Earth and Planetary Science Letters, v. 32, n. 1, p. 91–106, https://doi.org/10.1016/0012-821X(76)90189-8
Spencer, J. E., 1996, Uplift of the Colorado Plateau due to lithosphere attenuation during laramide low-angle subduction: Journal of Geophysical Research-Solid Earth, v. 101, n. B6, p. 13595–13609, https://doi.org/10.1029/96JB00818
Spiegel, C., Kohn, B., Belton, D., Berner, Z., and Gleadow, A., 2009, Apatite (U-Th-Sm)/He thermochronology of rapidly cooled samples: The effect of He implantation: Earth and Planetary Science Letters, v. 285, n. 1–2, p. 105–114, https://doi.org/10.1016/j.epsl.2009.05.045
Stern, T. W., Newell, M. F., Kistler, R. W., and Shawe, D. R., 1965, Zircon Uranium-Lead and Thorium-Lead Ages and Mineral Potassium-Argon Ages of La Sal Mountains Rocks, Utah: Journal of Geophysical Research, v. 70, n. 6, p. 1503–1507, https://doi.org/10.1029/JZ070i006p01503
Tork Qashqai, M., Carlos Afonso, J., and Yang, Y., 2016, The crustal structure of the Arizona Transition Zone and southern Colorado Plateau from multiobservable probabilistic inversion: Geochemistry, Geophysics, Geosystems, v. 17, n. 11, p. 4308–4332, https://doi.org/10.1002/2016GC006463
Van Wijk, J. W., Baldridge, W. S., van Hunen, J., Goes, S., Aster, R., Coblentz, D. D., Grand, S. P., and Ni, J., 2010, Small-scale convection at the edge of the Colorado Plateau: Implications for topography, magmatism, and evolution of Proterozoic: Lithosphere, v. 38, n. 7, p. 611–614, https://doi.org/10.1130/G31031.1
Vermeesch, P., and Tian, Y., 2014, Thermal history modelling: HeFTy vs. QTQt: Earth Science Reviews, v. 139, n. C, p. 279–290, https://doi.org/10.1016/j.earscirev.2014.09.010
Wernicke, B., 2011, The California River and its role in carving Grand Canyon: GSA Bulletin, v. 123, n. 7-8, p. 1288–1316, https://doi.org/10.1130/B30274.1
Whipp Jr., D. M., and Ehlers, T. A., 2007, Influence of groundwater flow on thermochronometer-derived exhumation rates in the central Nepalese Himalaya: Geology, v. 35, n. 9, p. 851–854, https://doi.org/10.1130/G23788A.1
Winn, C., Karlstrom, K. E., Shuster, D. L., Kelley, S., and Fox, M., 2017, 6 Ma age of carving Westernmost Grand Canyon: Reconciling geologic data with combined AFT, (U–Th)/He, and $^{4}He/^{3}He$ thermochronologic data: Earth and Planetary Science Letters, v. 474, p. 257–271, https://doi.org/10.1016/j.epsl.2017.06.051
Witkind, I. J., 1964, Geology of the Abajo Mountains Area San Juan County, Utah: United States Geological Survey Professional Paper 453, 117 p., https://doi.org/10.3133/pp453
Young, R. A., 2001, The Laramide-Paleogene history of the western Grand Canyon region: Setting the stage, *in* Young, R. A., and Spamer, E. E. editors, Colorado River Origin and Evolution: Grand Canyon, Arizona, Grand Canyon Association Monograph 12, p. 7–16.
Young, R. A., and Hartman, J. H., 2014, Paleogene rim gravel of Arizona: Age and significance of the Music Mountain Formation: Geosphere, v. 10, n. 5, p. 870–891, https://doi.org/10.1130/GES00971.1
Zhang, P., Molnar, P., and Downs, W. R., 2001, Increased sedimentation rates and grain sizes 2–4 Myr ago due to the influence of climate change on erosion rates: Nature, v. 410, p. 891–897, https://doi.org/10.1038/35073504